bioRxiv preprint doi: https://doi.org/10.1101/661751; this version posted June 7, 2019. The copyright holder for this preprint (which was not certified by peer review) is the author/funder, who has granted bioRxiv a license to display the preprint in perpetuity. It is made available under aCC-BY-NC-ND 4.0 International license.

The Role of Adaptation in Generating Monotonic Rate Codes in Auditory Cortex

Jong Hoon Lee[1,2], Xiaoqin Wang[1], Daniel Bendor[2]

[1] Laboratory of Auditory Neurophysiology, Department of Biomedical Engineering, Johns Hopkins University School of Medicine, Baltimore, MD, USA

[2] Institute of Behavioural Neuroscience, Department of Experimental Psychology, University College London, London, United Kingdom

Abstract

In primary auditory cortex, slowly repeated acoustic events are represented temporally by phase-locked activity of single neurons. Single-unit studies in awake marmosets (Callithrix jacchus) have shown that a sub-population of these neurons also monotonically increase or decrease their average discharge rate during stimulus presentation for higher repetition rates. Building on a computational single-neuron model that generates phase-locked responses with stimulus evoked excitation followed by strong inhibition, we find that stimulus-evoked short-term depression is sufficient to produce synchronized monotonic positive and negative responses to slowly repeated stimuli. By exploring model robustness and comparing it to other models for adaptation to such stimuli, we conclude that short-term depression best explains our observations in single-unit recordings in awake marmosets. Using this model, we emulated how single neurons could encode and decode multiple aspects of an acoustic stimuli with the monotonic positive and negative encoding of a given stimulus feature. Together, our results show that a simple biophysical mechanism in single neurons can allow a more complex encoding and decoding of acoustic stimuli.

Introduction

Our ability to discriminate complex sounds such as music [1,2], speech [3,4], and conspecific vocalizations [5], relies on the auditory system's analysis of an acoustic signal's spectral and temporal structures. For sequences of brief sounds, the timing of each acoustic event is explicitly encoded by the stimulus-locked activity of neurons throughout the ascending auditory pathway. In primary auditory cortex (A1), neurons can temporally lock to individual acoustic events up to around 40-50 Hz [6-10], matching the upper limit of acoustic flutter (the percept of a sequence of discretely occurring events). While repetition rates within the perceptual range of acoustic flutter are represented by A1 neurons with phase-locked activity, some of these neurons can also simultaneously vary their firing rate by monotonically increasing (*Sync*+) or decreasing (*Sync*-) firing rate over the range of repetition rates that span the range of flutter perception [11]. Temporal coding provides a faithful, unambiguous representation of the timing of acoustic events. However it must be analysed across time to determine the repetition rate of the stimulus. Rate coding, on the other hand, provides a more "processed" and instantaneous readout of repetition rate. Although rate coding is more ubiquitous in brain regions downstream from auditory cortex, one potential issue is that rate coding is used to represent multiple acoustic features in auditory cortex. For example, in a typical auditory cortical neuron, an increase in firing rate could represent a change in frequency, sound level [12], and/or sound location [13] In order for rate coding to be useful to downstream brain regions, neural circuits must be able to demultiplex concurrently encoded acoustic features.

In multiple brain regions, rate coding takes the form of positive and negative monotonic tuning. This form of opponent coding (positive/negative sloped rate relationship with a stimulus parameter) has been postulated to provide a number of advantages as an encoding strategy, including robustness to rate changes resulting from adaptation, allowing for the multiplexing of additional information within an overlapping rate code, and increasing the accuracy of extracting this information by reducing positively correlated noise between neurons [14]. How could the brain generate these types of neural representations? To explore this question, we used a leaky integrate-

bioRxiv preprint doi: https://doi.org/10.1101/661751; this version posted June 7, 2019. The copyright holder for this preprint (which was not certified by peer review) is the author/funder, who has granted bioRxiv a license to display the preprint in perpetuity. It is made available under aCC-BY-NC-ND 4.0 International license.

and-fire computational model of a neuron. Previously, we have used a similar modelling approach to generate stimulus synchronized responses to acoustic pulses in the range of flutter perception, by varying the delay and relative strength of excitatory and inhibitory inputs [15]. In this E-I (excitation-inhibition) based computational model, synchronized responses to slowly repeating sounds occur when inhibition is both stronger than and delayed relative to excitation. Building on this model, Gao et al (2016) [16] added a simplified adaptation mechanism to stimulus repetition rate, resulting in synchronized responses and non-synchronized monotonic positive and negative responses, but stimulus repetition rate ranged beyond acoustic flutter. The integration of rate coding in synchronizing neurons, to generate Sync+ and Sync- responses within the perceptual range of flutter, has not yet been directly examined using such computational models. Here we investigated the underlying neural mechanisms responsible for Sync+ and Sync- responses in auditory cortex and demonstrate that the addition of synaptic depression to the E-I model is sufficient to reproduce these two response modes - specifically stronger synaptic depression of excitatory inputs relative to inhibitory inputs leads to the Sync- response while weaker synaptic depression of excitatory inputs relative to inhibitory inputs leads to the Sync+ response. Using this model, we examined how a downstream neuron can combine Sync+ and Sync- inputs to effectively demultiplex a rate code such that discharge rate only monotonically varies with a single acoustic parameter.

Results

We first examined whether the E-I model described by Bendor (2015) [15] was capable of generating both Sync+ and Sync- responses to acoustic pulse trains, using the model's three existing independent parameters: The E/I ratio (the strength of excitatory input divided by the strength of the inhibitory input), the I-E delay (the temporal lag between the excitatory and inhibitory input), and the overall strength of excitation (Fig.1a). In this model, the number of spikes produced by each acoustic event was determined by the net excitatory input. If the number of spikes produced by each acoustic event did not change with repetition rate, neurons linearly increased their discharge rate with increasing repetition rate (Sync+). However, because the strength of lagging inhibition can decrease the overall net excitation in a repetition rate dependent manner, Sync- responses could be created at very high I/E ratios. While we observed that Sync+ responses were generated over a wide range of biologically plausible excitation and inhibition strengths (Fig1.c-e), Sync- responses could only be generated using biologically unrealistic I/E ratios, using a 3-fold increase in the strength of inhibition relative to excitation reported in intracellular recordings [17]. Although discharge rate decreased with increasing repetition rate for these modelled Sync- neurons, their rate responses were non-significant (firing rate below 2 std above mean spontaneous rate, see methods for details.), in contrast to the driven responses observed real Sync- neurons (Bendor and Wang 2007 [11], Fig.1c).

Fig 1. **Computational model of an auditory cortical neuron.** (A.) Simulated neural responses to an acoustic click train (top). each click was converted to an excitatory and inhibitory conductance input in our computational model, using an alpha function with a time constant of 5 ms (middle). Three parameters could be altered (I-E delay, E input and I/E ratio). Spikes were generated when membrane voltage reached a threshold (bottom). (B.) Cartoon of monotonic positive and negative responses. Monotonic positive neural responses increase the average discharge rate for stimuli with higher repetition rate. Monotonic negative responses decrease average discharge rate for stimuli with higher repetition rate. (C-E.) Examples of simulated neurons. Average discharge rate for increasing stimuli repetition rate for two example neurons. Model parameters for both neurons are the following: Neuron example 1 (C.): Excitatory input = 2 nS, Inhibitory input = 10 nS. Neuron example 2 (D.): Excitatory input = 4.5 nS, Inhibitory input = 8.5 nS. Error bars indicate s.e.m. (E) classification of neuron type across two parameters (Excitatory input and Inhibitory input) with a fixed I-E delay of 5 ms. The arrows indicate the parameters used for the example neurons (left arrow for example 1, right arrow for example 2). Shaded area indicates biologically plausible values where the I/E ratio is between 1.4 and 2.0.

Modelling short-term depression

We next examined how the E-I model could be modified to more accurately represent the repetition rate tuned responses of Sync+ and Sync- neurons. One possible mechanism that can vary discharge rate in a repetition

bioRxiv preprint doi: https://doi.org/10.1101/661751; this version posted June 7, 2019. The copyright holder for this preprint (which was not certified by peer review) is the author/funder, who has granted bioRxiv a license to display the preprint in perpetuity. It is made available under aCC-BY-NC-ND 4.0 International license.

rate sensitive manner is synaptic short-term plasticity, in particular, **short-term depression** (**STD**). If such adaptation is present, real neurons should decrease their firing rate between the start and the end of stimulus presentation. This difference would be larger for higher repetition rates, and a strong but short-term adaptation would be able to suppress the activity for high repetition rates without affecting responses for low repetition rates. Indeed, we observed that the number of spikes in real neurons at each acoustic event showed a decrease between the start and the end of stimuli sets for both Sync- and Sync+ real neuron populations (Fig.2a-c). Higher repetition rates showed a larger decrease for Sync- neurons than for lower repetition rates, the largest decrease seen at 48Hz ,the upper limit of acoustic flutter (Wilcoxon rank sum test, P <<0.001), whereas no decrease was observed at 8Hz, the lower limit of acoustic flutter (Wilcoxon rank sum test, P = 0.1) (Fig.2e). Similar to Sync- neurons, the decrease was present for Sync+ neurons at 48Hz (Wilcoxon rank sum test, P = 0.03) and absent at 8Hz (Wilcoxon rank sum test, P = 0.71) (Fig. 2f). When comparing this decrease between Sync- and Sync+ neurons for the same stimulus, we observed no significant difference for stimuli from 8 to 16Hz, and a significant difference from 20 to 48Hz (Supp Fig. 2a). Moreover, this depression in the neural response was stronger in the early portion of the acoustic stimulus (compared to the latter portion), and for Sync- neurons (compared to Sync+ neurons) (Fig.2a, S1 Fig). Sync+ neurons showed a weak global depression throughout stimulus presentation, and the profile of depression was not affected by repetition rate (Fig.2a, S1 Fig). Finally, the average number of spikes per acoustic event decreased monotonically (Spearman correlation coefficient: 0.99, P <0.001) for higher repetition rate in Sync- neurons, but not in Sync+ neurons (Spearman correlation coefficient = 0.36, P = 0.36.) (Fig.2d). Together, these observations suggest that adaptation to repeated stimuli was stronger for Sync- neurons than for Sync+ neurons (S2-S3 Figs)

Fig 2. Event-related activity of monotonic Sync neurons. (A-C.) Normalized number of spikes at each acoustic event for real Sync- (n = 27) and Sync+ (n = 26) neurons at 48Hz (a.) 24Hz (B.) and 8Hz (C.). Each data point was calculated by averaging the number of spikes at the time of each acoustic event (with response latency considered). Error bars indicate s.e.m. Black bar indicates stimulus presentation period. (D.) Average number of spikes of real Sync+ and Sync- neurons at each acoustic event across different repetition rates. **Sync+** : Spearman correlation coefficient = 0.36, P = 0.36 ; **Sync-** : Spearman correlation coefficient: 0.99, P <0.001. (E -F.) adaptation between first and last acoustic event of stimulus for Sync- (E.) and Sync+ (F.) neurons. (E.) adaptation at 8Hz (Wilcoxon rank sum test, P = 0.1), 24Hz (Wilcoxon rank sum test, P << 0.001), 48Hz (Wilcoxon rank sum test, P << 0.001). (F.) adaptation at 8Hz (Wilcoxon rank sum test, P = 0.71), 24Hz (Wilcoxon rank sum test, P = 0.01), 48Hz (Wilcoxon rank sum test, P = 0.03).

Model parameters. To add short term depression to our previous model, we introduced two additional parameters; the amplitude of depression ($\boldsymbol{A_D}$) which determined the strength of adaptation after each acoustic pulse, and the time constant of recovery ($\boldsymbol{\tau_P}$) which controlled how stimulus repetition rate affected adaptation during stimulus presentation (Fig.3a)(see methods for details). To control the strength of depression in our modified E-I model, we independently varied these two parameters for both excitatory and inhibitory inputs. We observed that by varying these two parameters, we were able to produce Sync+ (Spearman correlation coefficient $\rho > 0.8$, $P < 0.05$) and negative ($\rho < -0.8$, $P < 0.05$) responses (Fig.3b-d, see Methods). To further study the effects of these parameters, we first calculated the probability of obtaining monotonic positive (Fig.3b) or negative (Fig.3c) neurons across all values of $\boldsymbol{A_D}$ for a given set of time constants $\{\boldsymbol{\tau_{pE}}, \boldsymbol{\tau_{pI}}\}$ within a naturalistic range (between 0.05s and 0.2s). This was determined so that with values in the middle of the range, neurons would show no or very little depression for repetition rates under 8Hz, which corresponded to a time interval greater than 0.125s between two pulses. The average monotonicity index of model neuron responses across all values of $\boldsymbol{A_D}$ was highest for high $\boldsymbol{\tau_{pI}}$ and low $\boldsymbol{\tau_{pE}}$ values, and lowest for low $\boldsymbol{\tau_{pI}}$ and high $\boldsymbol{\tau_{pE}}$ values (Fig.3b-c). For a given set of time values { $\boldsymbol{\tau_{pE}}$ = 0.15, $\boldsymbol{\tau_{pI}}$= 0.10} we were able to obtain Sync+ neurons with strong depression and weak inhibition. The converse was true for Sync- neurons, where depression was stronger for excitation than inhibition (Fig.3d). In our parameter range, depression of excitation was more important than depression of inhibition in determining whether a neuron would be monotonic positive or negative. In this computational model, as in the previous model [15], the initial onset response was determined by the strength of excitation and inhibition, but not affected by synaptic depression. Values for excitatory and inhibitory input were chosen so that the onset response was on average between 40 and 60 spikes per second to match onset responses observed in real neurons [11], although different amplitudes of onset response did not affect our observations (S4 Fig).

bioRxiv preprint doi: https://doi.org/10.1101/661751; this version posted June 7, 2019. The copyright holder for this preprint (which was not certified by peer review) is the author/funder, who has granted bioRxiv a license to display the preprint in perpetuity. It is made available under aCC-BY-NC-ND 4.0 International license.

Fig 3. **Computational model of an auditory cortical neuron with short term depression.** (A.) At each acoustic signal (top) we simulate the decrease in the probability of release of synaptic vesicles with an amplitude of A_D followed by an exponential recovery with time constant τ_p (middle top) (See methods for details). This probability of release then determined the amplitude of conductance input to our model neuron (middle bottom). a decrease in conductance amplitude during stimuli presentation (black bar) resulted in a decrease in discharge rate per acoustic signal (bottom). (B-D.) Adaptation parameter space. Average positive (B.) and negative (C.) monotonicity index for a given set of recovery time constants $\{ \tau_{pE}, \tau_{pI} \}$. Average monotonicity index at $\{\tau_{pE} = 0.15, \tau_{pI} = 0.10\}$ for different values of A_{DE} and A_{DI} (D.).

For our simulated neurons, A_D values were determined so that simulated Sync+ and Sync- neurons matched real neurons in both trial-by-trial spiking activity (Fig.4) and average population activity (Fig.5). Monotonicity was significant for both Sync+ (Spearman correlation coefficient $\rho = 0.91$, $P < 0.001$) and Sync- ($\rho = 0.85$, $P = 0.012$) simulated neurons (Fig.5e,f), and temporal fidelity over the range of repetition rates spanning flutter perception was maintained despite adaptation (Vector Strength (VS)>0.1, and Rayleigh statistic>13.8, $P < 0.001$).

Fig 4. Real and Simulated monotonic Sync example neurons. Raster plot comparison between simulated Sync+ (B; $A_{DE} = 0.4$, $A_{DI} = 0.1$, $\tau_{pE} = 0.15$ s $\tau_{pI} = 0.10$ s.) and Sync- (D; $A_{DE} = 0.1$, $A_{DI} = 0.4$, $\tau_{pE} = 0.15$ s $\tau_{pI} = 0.10$ s.) neurons with real Sync+ (C; unit m32q-337) and Sync- (E; unit m32q-29) neuron examples. the black bar indicates the time during when stimuli was given as input. $A_{DE} = 0.4$, $A_{DI} = 0.1$, $\tau_{pE} = 0.15$ s $\tau_{pI} = 0.10$ s.

Fig 5. Monotonicity of real and simulated neurons. Comparison between simulated and real neuron population PSTH for Sync+ (A; n = 30, B; n = 26) and Sync- (C; n = 30, D; n = 27) neurons. (E, F.) Normalized discharge rate for Sync + and Sync- neurons across stimuli with different repetition rates. Discharge rate was normalized to the maximum value across stimuli. (E.) Population average of real Sync+ and Sync- neurons. (F.) Population average of simulated Sync+ and Sync- neurons.

Model robustness. Next, we examined the robustness of our model to different types of noise. Our computational model operated, as did the previous model [15], with a fixed spontaneous rate (~4 spk/s) comparable to that of our real neuron data (median spontaneous rate = 3.8 spk/s). This was generated by adding Gaussian noise to the baseline excitatory and inhibitory conductances of the neuron (see methods). Increasing the amplitude of noise also increased the spontaneous rate (Fig.6a). We examined how robust our model was for varying noise amplitude and observed that it did not affect monotonicity for both Sync+ and Sync- simulated neurons (Fig.6b). Vector Strength was less robust to changes in noise amplitude, in particular for Sync- simulated neurons, where low noise amplitude resulted in a complete lack of stimulus synchrony for high repetition rates (Fig.6d, e), due to the evoked responses consisting of an onset followed by suppression. Our model also included temporal jitter (Fig.6c) to emulate more realistic responses, by adding Gaussian noise to the timings of each acoustic pulse. Similar to the conductance noise amplitude, changes to temporal jitter did not affect monotonicity. We also observed that the vector strength in Sync- simulated neurons was more affected by temporal jitter than for Sync+ simulated neurons (Fig 6f, g). However, with the exception of Sync- simulated neurons with strong temporal jitter (above 7 s.d.) these simulations in the presence of noise could still be classified as synchronised monotonic responses (see methods for criteria). We further explored model robustness by studying how input parameters such as excitation and inhibition amplitude affected monotonicity and vector strength. Monotonicity in Sync+ simulated neurons did not seem to be affected by changes in these parameters (Fig.7a). In Sync- neurons however, the monotonicity index was reduced to 0 for IE ratios under 1.0 (Fig.7b). In addition, for stronger excitatory input amplitudes the model required higher IE ratios to produce monotonic negative responses. As for vector strength, both Sync+ and Sync- simulated neurons showed a weak decrease in stimulus synchrony for excitatory input amplitudes under 2nS (Fig.7c, d).

bioRxiv preprint doi: https://doi.org/10.1101/661751; this version posted June 7, 2019. The copyright holder for this preprint (which was not certified by peer review) is the author/funder, who has granted bioRxiv a license to display the preprint in perpetuity. It is made available under aCC-BY-NC-ND 4.0 International license.

Fig 6. Model robustness. Spontaneous rate in relation to noise amplitude (A.) Monotonicity in Sync+ and Sync- neurons in relation to noise amplitude (B.) and temporal jitter (C.) Vector strength in relation to noise amplitude in Sync+ (D.) and Sync- (E.) neurons, and in relation to temporal jitter in Sync+ (F.) and Sync- (G.) neurons.

Fig 7. Model robustness regarding Excitation and Inhibition amplitude. Average monotonicity index (A, B.) and average vector strength (C, D.) across different values for recovery time constants $\{ \tau_{pE}, \tau_{pI} \}$ ranging between 0.06 and 0.20s for a given value of $\{ A_{DE}, A_{DI} \}$. When within the parameters of producing Sync+ neurons, Monotonicity is unaffected by changes in E strength and IE ratio (A.). For parameters resulting in Sync- neurons, Monotonicity is negative only when inhibition is stronger than excitation (IE ratio larger than 1) (B.). Vector strength is maintained for E strength above 2nS and is minimally affected by IE ratio in both scenarios (C, D.).

Different mechanisms for adaptation to repeated acoustic pulses. So far in this study we explored short-term depression as a possible underlying mechanism for Sync+ and Sync- neurons observed in A1. Next, we explored other possible mechanisms that may allow neurons to adapt to acoustic pulse trains and compared their effects to that of our short-term depression model. One such mechanism is **short-term facilitation (STF)**; the adaptation of neural activity during stimulus presentation for higher repetition rates could arise from facilitation of inhibition, as opposed to depression of adaptation. We thus modelled short-term facilitation using the same parameters as short-term depression. However, instead of decreasing the probability of release (and therefore the conductance input amplitude), this probability was increased at each acoustic input until it was recovered back to its initial value (Fig.8) (see methods). When combining depression of excitation and facilitation of inhibition, the model was able to produce both Sync+ and Sync- responses. Similar to our original model (depression of excitation and inhibition) depression of excitation was the determining factor for the direction of monotonicity for simulated neurons (Fig.8a, b). However, increasing the strength of facilitation in the inhibitory input lead to a decrease in the monotonicity slope of Sync+ neurons and an increase in the monotonicity slope of Sync- neurons. When both excitation and inhibition were facilitated, all simulated neurons were Sync+ neurons (Fig.8c, d). In the case where there was strong facilitation of inhibition and weak depression of excitation, our model produced non-monotonic synchronized responses (highest discharge rates in the middle of the acoustic flutter range).

Fig 8. Computational model including short term facilitation. Short term facilitation was added to the model by increasing the probability of release (see methods) at each acoustic input, which would decay back to the initial value with a time constant τ_p. Initial probability of release was 0.5 compared to 1.0 in short term depression model to compensate for changes in conductance input amplitudes. (A, B.) Depression of excitation and facilitation of inhibition. (C, D.) Facilitation of both excitation and inhibition. (A, C.) average monotonicity index for a given value of adaptation amplitude A_D, for time constants $\{ \tau_{pE}, \tau_{pI} \}$ ranging between 0.06 and 0.20s. (B, D.) discharge rates for example neurons. (B.) Simulated neurons with depression of excitation and facilitation of inhibition. Example neuron 1 at $\{ A_{DE} = 0.1, A_{DI} = -0.0\}$, Spearman correlation coefficient = 0.76, P = 0.01. Example neuron 2 at $\{A_{DE} = 0.1, A_{DI} = -0.4\}$, Spearman correlation coefficient = 0.25, P = 0.45. Example neuron 3 at $\{A_{DE} = 0.3, A_{DI} = -0.0\}$, Spearman correlation coefficient = -0.66, P = 0.03 Example neuron 4 at $\{A_{DE} = 0.3, A_{DI} = -0.4\}$, Spearman correlation coefficient = -0.74, P = 0.01 (D.) Simulated neurons with facilitation of both excitation and inhibition. Example neuron 1 at $\{ A_{DE} = -0.2, A_{DI} = -0.2\}$, Spearman correlation coefficient = -1, P << 0.001. Example neuron 2 at $\{A_{DE} = -0.0, A_{DI} = -0.4\}$, Spearman correlation coefficient = 0.07, P = 0.84. Time constants of all example neurons: $\{\tau_{pE} = 0.15, \tau_{pI} = 0.10\}$

Another possible mechanism for adaptation to stimulus statistics is **spike-frequency adaptation** (**SFA**). Although the time scale for SFA is generally much shorter than that of short-term depression [18. 19], the two effects could be complimentary. In order to separate SFA from our observations, we studied Inter-Spike Intervals (**ISIs**) at onset for both Sync+ and Sync- real neurons by comparing the difference between the first and second ISI and second and third ISI (S5 Fig). Within the same population, we observed a significant difference between the first, second and third ISI (KS test, P <0.05), and thus the presence of SFA. However, the time scale of SFA was in the order of 0.5ms, compared to the time scale of flutter (20 to 250ms). In addition, SFA at the onset

bioRxiv preprint doi: https://doi.org/10.1101/661751; this version posted June 7, 2019. The copyright holder for this preprint (which was not certified by peer review) is the author/funder, who has granted bioRxiv a license to display the preprint in perpetuity. It is made available under aCC-BY-NC-ND 4.0 International license.

between Sync+ and Sync- neurons was significantly different (t-test, $P<0.05$) but the difference was in the order of 1ms.

To further compare the aforementioned mechanisms between each other and with real neurons populations, we studied the strength of adaptation in relation to discharge rate at different time windows during the stimulus presentation (acoustic pulse train with a repetition rate of 40Hz). The strength of adaptation, equivalent to the amplitude of adaptation $\mathbf{A_D}$ shown in the model above, was defined as the firing rate during the time window spanning the given acoustic pulse divided by the firing rate during the previous acoustic pulse. Real neurons with firing rates lower than the spontaneous rate during the first 2 pulses (5/27 neurons in Sync-, 7/26 neurons in Sync+) were excluded from analysis. The strength of adaptation was also calculated for models with different mechanisms for adaptation; the base model with STD for excitation and inhibition, the base model with additional weak or strong SFA (see methods), and the facilitation model with STD for excitation and STF for inhibition (Fig.9a). As expected, adaptation during the first to second pulse for Sync- simulated neurons was strongest in the strong SFA model, and weakest in the facilitation model. Adaptation increased significantly between first to second pulse and first to third pulse for the base model and for the facilitation model (Wilcoxon sign rank test $P <<0.001$) but not for models with weak or strong SFA (Wilcoxon signed rank test $P = 0.06$ and $P = 0.5$ respectively). For Sync+ neurons, all models showed a weak or non-significant adaptation. In the case of real Sync- neurons, most neurons showed significant depression between the first and second pulse (18/22 neurons, median = 0.59, t-test, $P << 0.001$) and between first and third pulse (18/22 neurons, median = 0.90, $P << 0.001$) (S6 Fig), and the difference of adaptation strength between these two time windows was statistically significant (paired Wilcoxon rank sum test, $P < 0.01$) (Fig.9b) these results were most comparable to our base model using only short-term depression. As for Sync+ neurons, individual responses showed both depression and facilitation during onset. 9/19 neurons and 8/19 neurons showed depression between 1st and 2nd pulses and between 1st and 3rd pulses respectively (median = 0 for both, Wilcoxon signed rank test, $P > 0.05$) (Fig. 9b). These results showed that short-term depression was sufficient to reproduce adaptation to acoustic pulse trains in real Sync+ and Sync- neurons.

Fig 9. Adaptation between individual synaptic inputs for real neurons and different models. (A.) Adaptation between the 1st and 2nd input, and between 1st and 3rd input for Sync+ and Sync- neurons for models with different adaptation mechanisms. Strength of adaptation increased significantly between 1st to 2nd pulse and 1st to 3rd pulse for Sync- base and facilitation model (paired Wilcoxon signed rank test $P << 0.001$) (B.) Strength of adaptation in real Sync+ and Sync- neurons between the 1st and 2nd input, and between 1st and 3rd input. Strength of adaptation increased significantly between 1st to 2nd pulse and 1st to 3rd pulse for Sync- neurons (Wilcoxon signed rank test $P <0.01$). Asterisks directly above bars indicate that the adaptation amplitude was significantly different from 0 (Wilcoxon signed rank test $P <0.05$).

Response to pure tones. If we consider pure tones to be similar to acoustic pulse trains with a very high repetition rate, the responses these stimuli evoke in Sync+ neurons and Sync- neurons would be different. We would more likely observe a brief onset response in Sync- neurons compared to a more sustained response observed in sync+ neurons. Using our computational model, we could also emulate responses of Sync+ and Sync- neurons to different sets of stimuli such as pure tones. In real neurons, similar responses were evoked by pure tones (at the neuron's best frequency) and pulse trains with high repetition rates (Fig.10a): We observed an onset followed by a sustained response for Sync+ neurons and an onset followed by a suppressed response for Sync- neurons. Both our computational model for Sync+ and Sync- neurons behaved similarly to real neurons (Fig.10b), with Sync- simulated neurons showing a transient onset followed by suppressed response, whereas Sync+ showed a sustained response during stimulus. Our simulated responses to pure tones did however differ with real neuron response dynamics (S7 Fig). Sync + responses were greatly exaggerated in our simulated neurons compared to real neurons, with the peak response time being significantly later than onset response time. Decreasing the initial excitatory input amplitude or introducing SFA to the model seem to affect Sync- responses, however increasing the excitation strength led to a proportional increase in onset response (S8 Fig). These data suggest that the temporal profile of pure-tone responses could be used to predict whether a neuron is Sync+ or Sync-, even though actual firing rates of the base model did not accurately reflect real neuronal responses. We tested this prediction by measuring the median of all spike times during stimulus presentation of pure tone responses in real and simulated neurons: Neurons with sustained responses would have a higher median spike time during stimulus presentation than those showing onset responses. This was indeed the case for both real neuron populations (Fig.10c) (median spike time

bioRxiv preprint doi: https://doi.org/10.1101/661751; this version posted June 7, 2019. The copyright holder for this preprint (which was not certified by peer review) is the author/funder, who has granted bioRxiv a license to display the preprint in perpetuity. It is made available under aCC-BY-NC-ND 4.0 International license.

of Sync+ neurons = 89ms, median spike time of Sync- neurons 44ms, Wilcoxon rank sum test, $P < 0.05$) and simulated neurons (S8 Fig). Results for Sync+ simulated neurons suggest that median spike times during the stimulus varies depending on the strength of adaptation whereas for Sync- neurons it stays constant. This could explain the variation of median spike times in real Sync+ neurons compared to Sync- neurons (Fig.10c).

Fig 10. Pure tone responses. Normalized responses to pure tones in real (A; Sync +, n =26. Sync-, n = 27) and simulated neurons (30 simulated neurons). Normalized spike rate was obtained by dividing the population average response to the average peak response during stimulus presentation. (C.) Distribution of median spike times during stimuli presentation of all Sync+ neurons (green asterisk: median of distribution= 89ms) and Sync- neurons (yellow asterisk: median of distribution= 44ms). The two distributions were significantly different (Wilcoxon rank sum test, $P < 0.001$).

Encoding and decoding multiple acoustic features. Sync+ and Sync- neurons dually represent the repetition rate of acoustic flutter through monotonic discharge rate and through stimulus-synchronized activity [11]. However, how downstream neurons read out this information, especially in the context of additional concurrently encoded acoustic parameters is unknown. To further explore this issue, we added a monotonic modulation of firing rate in our model, to reflect a stimulus' sound level [12,20,21] and emulate multiplexing of different acoustic features in firing rate. Our Sync+ and Sync- neurons therefore varied their firing rates to both stimulus repetition rate and sound amplitude (Fig.11b, c). We speculated that these two parameters could be "demultiplexed" by simply adding or subtracting Sync+ and Sync- responses from each other. Subtracting Sync- responses from Sync+ responses, generated a firing rate that was insensitive to changes in stimulus amplitude, providing a robust monotonic change in firing rate to repetition rate (Fig.11d, e). Using the opposite approach and summing Sync+ and Sync- responses created an invariant response to repetition rate while preserving the monotonic tuning to stimulus amplitude (Fig.11f, g).

Fig 11. Opponent coding with Sync+ and Sync- neurons. (A.) Cartoon of the effect of stimulus amplitude to Sync+ and Sync- tuning curves in relation to stimulus repetition rate. Higher sound levels shift the tuning curves towards higher firing rates. (B, C.) Normalized firing rate for a given stimulus with two varying parameters, stimulus amplitude and stimulus repetition rate for Sync+ and Sync- simulated neurons respectively. Cartoon (D.) and model output (E.) illustrating tuning curves in relation to stimulus repetition rate and amplitude when subtracting Sync- responses from Sync+ responses. Changes in activity reflects changes in repetition rate but not in stimulus amplitude. Cartoon (F.) and model output (G.) illustrating tuning curves in relation to stimulus repetition rate and amplitude when adding Sync- responses to Sync+ responses. Changes in activity reflects changes in stimulus amplitude but not in repetition rate.

We quantified this further by comparing the mutual information (MI) between firing rate and each stimulus feature with our simulations. We observed that subtracting Sync- responses from Sync+ responses resulted in the most MI regarding stimulus repetition rate (Fig.12a), while having the least MI for stimulus amplitude, compared to other combinations (Fig.12b). This demonstrates that the difference in firing rates between Sync+ and Sync- neurons preserves the rate code for stimulus repetition rate while ignoring stimulus amplitude. Furthermore, MI for stimulus repetition rate was significantly higher when subtracting Sync- responses from Sync+ responses than only using Sync+ neurons, suggesting that this "demultiplexing" procedure can even lead to an enhancement of the rate code. If instead we summed the Sync+ and Sync- responses, we observed the opposite result- MI increased for stimulus amplitude and decreased for stimulus repetition rate. Thus the summation of firing rates between Sync+ and Sync- neurons preserves the rate code for stimulus amplitude while ignoring stimulus repetition rate. Altogether, these results indicate that more than one acoustic feature can be multiplexed together, by concurrently encoding each feature using a monotonically tuned rate code. However, it is critical to have both positive and negative monotonic tuning to at least one acoustic feature for this to work. Demultiplexing this information downstream only requires summing or subtracting firing rates between different groups of neurons, which is both mechanistically simple and biologically plausible.

bioRxiv preprint doi: https://doi.org/10.1101/661751; this version posted June 7, 2019. The copyright holder for this preprint (which was not certified by peer review) is the author/funder, who has granted bioRxiv a license to display the preprint in perpetuity. It is made available under aCC-BY-NC-ND 4.0 International license.

Fig 12. Mutual information and opponent coding. Mutual information (MI) between firing rate each stimulus feature: repetition rate (A.) and stimulus amplitude (B.) Mutual information was calculated (see methods) with different combinations of model neurons that had randomly distributed amplitude modulations added to their discharge rate. All categories were significantly different from each other (Kruskal-Wallis test with a post-hoc Wilcoxon rank sum test with Bonferroni correction)

Discussion

Here we describe a computational model able to reproduce the monotonically-tuned synchronized responses of auditory cortex neurons evoked by acoustic pulse trains in the range of flutter perception. By adding the parameters of pre-synaptic short-term depression to both the excitatory and inhibitory inputs of the initial conductance-based integrate-and-fire E-I model [15] we were able to model both positive and negative monotonically tuned, stimulus synchronized neurons (Sync+ and Sync-). Sync+ responses were generated when adaptation for excitation was weak or not present, whereas Sync- responses were generated when adaptation for excitation was strong. Adaptation of inhibition played a role in facilitating or supressing post-synaptic responses. This adaptation was modelled using a realistic set of time constants and rates of adaptation, consistent with previous studies across multiple laboratories [6,22,23-27]. When compared with other possible mechanisms for adaptation such as pre-synaptic short-term facilitation and post-synaptic spike-frequency adaptation, our model best emulated adaptation of real Sync+ and Sync- neurons to acoustic pulse trains in the perceptual range of flutter and was also able to make testable predictions such as temporal dynamics of responses to pure-tones, which was subsequently confirmed in our real neuronal population.

With this model, we were able to further explore the role of monotonic positive and negative encoding neurons in the auditory cortex. Multiple stimulus features other than repetition rate such as sound level [12] and sound source location [28] have shown monotonic rate coding. We demonstrated that the "segregation problem" of multiple stimulus features could be solved if one or more features were encoded by monotonic positive and negative rate code tuning. This "opponent coding" would isolate information originating from one feature from others. Although here we simulated Sync+ and Sync- neurons in auditory cortex, opponent coding of temporally modulated information has also previously been reported in the Secondary somatosensory cortex (S2) [29] for vibro-tactile stimuli.

Although primary somatosensory [8] and auditory cortices encode stimulus timing using both a rate and temporal representation, downstream neurons may only be processing one of these inputs. Mountcastle and colleagues [30] previously postulated that a neural mechanism could read out the periodic inter-spike intervals of the spike trains evoked in S1. In anesthetized animals, ISI does contain by far the highest amount of information, assisted by information from firing rate [31]. However multiple studies in awake animals [29,32-34] in both sensory areas have shown that firing rate, not precise spike timing, more accurately represents the psychophysical discrimination thresholds of stimulus repetition rate.

In the auditory pathway, we observe a loss of temporal fidelity to repetitive stimuli as we move along from the auditory periphery to cortex (e.g., cochlear nucleus: [35-38], inferior colliculus: [39-41] medial geniculate body: [23,42], auditory cortex: [8,9,43-45]) due to biophysical properties of neurons and temporal integration of converging inputs from one level to the next [37]. This loss of temporal fidelity in the auditory cortex, while problematic for a temporal representation, is mitigated by the substitution of a rate code for encoding the same information. Thalamic and prethalamic areas in the auditory pathway contain predominately synchronized neurons, while non-synchronized (nSync) neurons using firing rate to encode temporal information for repetition rates above the upper limit of flutter are most prevalent in auditory cortex (and to a limited extent the medial geniculate nucleus (MGB)) [42]. Both Sync and nSync neurons responding to flutter were found in A1 and in the Rostral fields (R and RT), although a higher proportion of Sync+/- neurons were found in A1, compared to R and RT where there were more nSync+/- neurons (monotonically encoding repetition rates within the range of flutter perception). Similar transformations were found in the Somatosensory pathway from Thalamus to S1, S2 [29] where, in the same manner as the auditory cortex, S2 neurons showed a much weaker stimulus-locking than S1 for vibrotactile stimuli and encoded temporal information using either positive or negative monotonic rate

bioRxiv preprint doi: https://doi.org/10.1101/661751; this version posted June 7, 2019. The copyright holder for this preprint (which was not certified by peer review) is the author/funder, who has granted bioRxiv a license to display the preprint in perpetuity. It is made available under aCC-BY-NC-ND 4.0 International license.

codes. Previous studies have suggested single-compartment computational models to explain this transformation of temporal encoding across the auditory system [15,22,46,47], but all of these studies have grouped synchronized neurons in a single rate-coding category, not distinguishing between positive/negative monotonic neurons. We postulate that monotonic synchronized neurons are an intermediary stage in the transformation of stimulus information encoding from a temporal representation to a rate code lacking stimulus locked responses.

There are, however, several caveats to our computational model. First, we compare single unit data from marmosets with simulated neurons using cellular parameters based on intra-cellular recordings of ketamine-anesthetized rats [22], due to the fact that no data exists for marmosets. Because ketamine is an NMDA antagonist, our model only simulated AMPA and GABA-A receptors, making no distinction between the two. NMDA receptors produce synaptic inputs with a longer time-constant (10-25ms) than AMPA and GABA-A receptors (5ms) and may thus explain the difference in response between awake and anesthetized animals. Previous studies have introduced NMDA receptors to single compartment models [15,46,47], but none have studied how it affects the monotonicity of synchronized responses.

Alongside acoustic pulse trains, Bendor and Wang [11,48,49] also recorded responses of the same neurons to sinusoidal amplitude modulated (SAM) tones and to pure tones. In the current model, an acoustic pulse is modelled as a single excitatory gaussian kernel followed by an inhibitory kernel. SAM tones have different spectral bandwidth and pulse duration depending on the modulation frequency [34] and cannot be represented accurately by our model. As for pure tone responses, our model represents the input as a net onset excitation followed by inhibition during stimulus presentation. Our model also considers that A1 neurons receive the same excitatory and inhibitory conductance input for each acoustic pulse regardless of the repetition rate. However, both in vitro [50] and in silico [46] studies show evidence for short-term plasticity to repetitive acoustic stimuli for projections from Inferior Colliculus (IC) to MGB neurons. Inputs to A1 neurons originating from acoustic pulses would have therefore passed such filters. While the addition of parameters that account for these different types of stimuli and transformations could provide further improvements to the model, our aim was to demonstrate that the addition of adaptation to a simple computational model is sufficient to produce positive and negative monotonic rate coding in stimulus-synchronizing neurons.

Methods

Ethics Statement. The electrophysiology data used in this study comprised of a previous published dataset [11] collected in the laboratory of Professor Xiaoqin Wang at Johns Hopkins University. All experimental procedures were approved by the Johns Hopkins University Animal Use and Care Committee and followed US National Institutes of Health guidelines.

Electrophysiological recordings and acoustic stimuli. Our electrophysiology data in this report comprised of previous published datasets [11]. For these datasets, the authors performed single-unit recordings with high-impedance tungsten micro-electrodes ($2–5M\Omega$) in the auditory cortex of four awake, semi-restrained common marmosets (Callithrix jacchus).

Action potentials were sorted on-line using a template-matching method (MSD, Alpha Omega Engineering). Experiments were conducted in a double-walled, soundproof chamber (Industrial Acoustic Co., Inc.) with 3-inch acoustic absorption foams covering each inner wall (Sonex, Illbruck, Inc.).

Acoustic stimuli were generated digitally (MATLAB- custom software, Tucker Davis Technologies) and delivered by a free-field speaker located 1 meter in front of the animal. Recordings were made primarily for the three core fields of auditory cortex (177/210 neurons)- primary auditory cortex (AI), the rostral field (R), and the rostrotemporal field (RT), with the remaining neurons recorded from surrounding belt fields. For each single unit isolated, the best frequency (BF) and sound level threshold was first measured, using pure tone stimuli that were 200 ms in duration. We next generated a set of acoustic pulse trains, where each pulse was generated by windowing a brief tone at the BF by a Gaussian envelope. Repetition rates ranged from 4Hz to 48Hz (in 4Hz steps) Acoustic pulse train stimuli were 500 ms in duration, and all intertrial intervals were at least 1 s long. Each stimulus was presented in a randomly shuffled order with other stimuli, and repeated at least five times for all neurons, and at least ten times for about 55% of neurons (115/210). Stimulus intensity levels for acoustic pulse

bioRxiv preprint doi: https://doi.org/10.1101/661751; this version posted June 7, 2019. The copyright holder for this preprint (which was not certified by peer review) is the author/funder, who has granted bioRxiv a license to display the preprint in perpetuity. It is made available under aCC-BY-NC-ND 4.0 International license.

trains were generally 10 – 30 dB above BF-tone thresholds for neurons with monotonic rate-level functions and at the preferred sound level for neurons with non-monotonic rate-level functions.

Computational model

Single neuron model.

The single unit model used in this study was based on the model published by Bendor 2015 [15]. A conductance-based leaky integrate-and-fire model was simulated using MATLAB using the following equation, using parameters obtained from Wehr and Zador 2003 [17]:

$$V_{t+1} = -\frac{dt}{C}[g_e(t)(V_t - E_e) + g_i(t)(V_t - E_i) + g_{rest}(t)(V_t - E_{rest}) + V_t + \sigma_s \omega_n \sqrt{\Delta t}$$

Each acoustic pulse was simulated as the summation of 10 excitatory and 10 inhibitory synaptic inputs [20], each temporally jittered (Gaussian distribution, σ = 1 ms). Each synaptic input was modelled as a time-varying conductance fit to an alpha function:

$$\alpha(t) = A(t)te^{-\frac{\tau}{\tau_s}}$$

When simulating neurons without short-term plasticity, A was determined by the excitatory or inhibitory input parameter and stayed constant throughout the simulation. This amplitude ranged between 0 to 6nS for excitatory inputs and 0 to 12nS for inhibitory inputs, as in Bendor 2015 [11]. A synaptic input delay was added to simulate the delay between peripheral auditory system and auditory cortex, and whereas in the previous study the temporal delay between excitatory and inhibitory inputs (I-E delay) was a variable, in this study it was fixed at 5 ms. In our model, an action potential occurred whenever the membrane potential of the model neuron reached a threshold value V_{th}. After the action potential, the potential was reset to a value E_{rest} below the threshold potential, $E_{rest} < V_{th}$.

Table 1. Fixed model parameters.

Membrane capacitance	$\boldsymbol{C}$	0.25nF
Leak membrane conductance	$\boldsymbol{g_{rest}}$	25nS
Excitatory reversal potential	$\boldsymbol{E_e}$	0mV
Inhibitory reversal potential	$\boldsymbol{E_i}$	-85mV
Alpha function time constant	$\boldsymbol{\tau_s}$	5ms
Synaptic input delay		10ms
I-E delay		0.1ms
Simulation timestep	$\boldsymbol{\Delta t}$	10mVs^{-1}
Scale of noise	$\boldsymbol{\sigma_s}$	[-1 :1]
Gaussian noise	$\boldsymbol{\omega_n}$	

Short-term plasticity: Depression. In order to introduce short-term plasticity in the model we regarded the probability of presynaptic release P_{rel} as a dynamic variable depending on the input stimuli (acoustic pulse trains) [51,52]. In the absence of presynaptic activity, the release probability decays exponentially back to its initial value P_0 with the following equation:

$$\tau_P \frac{dP_{rel}}{dt} = P_0 - P_{rel}(t)$$

Immediately after each stimulus input the release probability is reduced.

$$P_{rel}(t) \rightarrow (1 - A_D) * P_{rel}(t)$$

$$A(t) = A(0) * P_{rel}(t)$$

bioRxiv preprint doi: https://doi.org/10.1101/661751; this version posted June 7, 2019. The copyright holder for this preprint (which was not certified by peer review) is the author/funder, who has granted bioRxiv a license to display the preprint in perpetuity. It is made available under aCC-BY-NC-ND 4.0 International license.

Where A_D controls the amount of depression and $A(t)$ is the amplitude of conductance input at time t. Modelling synaptic depression consisted thus of 4 parameters: the recovery time constants for both excitatory and inhibitory synapses (τ_{pE}, τ_{pI}) ranging from 50 to 200ms, and the depression factor A_{DE} and A_{DI} ranging from 0 to 0.5. P_0 in this model was equal to 1. These values were consistent with intra-cellular recordings in previous studies [26,52].

Short-term plasticity: Facilitation. Short-term facilitation was added to the model using a similar model to that of short-term depression. In the case of facilitation, A_D varies between -0.5 and 0. Therefore, the probability of release $P_{rel}(t)$ Increases after each stimulus input, then decays back to the initial value. When modelling facilitation P_0 was equal to 0.5 so that the resulting amplitude of conductance remained comparable to that of short-term depression.

Spike-Frequency Adaptation. We modelled spike-frequency adaptation by including an addition current in the model.

$$V_{t+1} = -\frac{dt}{C}[g_e(t)(V_t - E_e) + g_i(t)(V_t - E_i) + g_{rest}(t)(V_t - E_{rest}) + g_{sra}(t)(V_t - E_K) + V_t + \sigma_s\omega_n\sqrt{\Delta t}$$

Where g_{sra} is the spike-frequency adaptation conductance modelled as a K^+ conductance [53] . When activated, this will hyperpolarize the neuron, slowing any spiking that may be occurring. The conductance relaxes to zero exponentially with the time constant τ_{sra} through the following equation:

$$\tau_{sra}\frac{dg_{sra}}{dt} = -g_{sra}$$

Whenever the neuron fires a spike, g_{sra} is increased by an amount Δg_{sra}, causing the firing rate to adapt in a sequence of steps in relation to the neurons spiking activity.

Data analysis

Classification of neurons, Synchrony. Two tests were used to determine whether a neuron was Sync or nSync: Vector strength (VS) and rate response. **Vector strength** (VS) was calculated for each repetition rate from 8 to 48Hz with the following equation:

$$VS = \frac{1}{N}\sqrt{\sin(\frac{2\pi t^{(n)}}{IPI})^2 + \cos(\frac{2\pi t^{(n)}}{IPI})^2}$$

$$RS = 2 * N * VS^2$$

Where N is the number of spikes, $t^{(n)}$ is the time of n^{th} pulse and IPI the interpulse interval. If vector strength was significant (Rayleigh statistic $RS > 13.8$) and above 0.1 for three consecutive repetition rates, and if the rate response was also considered significant (average discharge rate 2 s.d. above the mean spontaneous rate and an average of more than 1 spike per stimulus), then the neuron was considered Sync. If the rate response was significant but the neuron did not pass the synchrony criteria, it was considered nSync. In our dataset 125/210 neurons were classified as Sync.

Classification of neurons, Monotonicity. The monotonicity of the discharge rate for a given repetition rate was determined by calculating the Spearman correlation coefficient (ρ) for stimuli spanning from 8 to 48Hz. If coefficient was larger than 0.8 and statistically significant (p-value < 0.05) the neuron was considered positive monotonic. If the coefficient was smaller than -0.8 and statistically significant, the neuron was considered negative monotonic. Neurons satisfying neither of these criteria were considered non-monotonic. These three classification methods applied to both real and simulated neurons. In our dataset of real neurons, we found 126/210 monotonic neurons and 84 non-monotonic neurons.

bioRxiv preprint doi: https://doi.org/10.1101/661751; this version posted June 7, 2019. The copyright holder for this preprint (which was not certified by peer review) is the author/funder, who has granted bioRxiv a license to display the preprint in perpetuity. It is made available under aCC-BY-NC-ND 4.0 International license.

Classification of neurons, Sync+ and Sync- neurons. Based on the two classification criteria, we classified 25 Sync+ and 27 Sync- neurons with significant stimuli-driven responses.

PSTH. Individual peri-stimulus time histograms (PSTHs) were calculated by convolving a Gaussian kernel (σ = 10ms) with a neuron spike train. The population PSTH was calculated as a mean of individual PSTHs.

Mutual information analysis. The MI of stimulus frequency carried in the firing rate was computed for all Sync neurons across all stimuli. MI between frequency f and firing rate fr is given by the equation

$$I(f, fr) = \frac{1}{N_f} \sum_{r} p(fr|f) \log_2 \frac{P(fr|f)}{P(fr)}$$

Where $N_f = 12$ s the number of stimulus frequencies. To account for the fact that MI is positively biased [54-55]. the values were linearly extrapolated to a resolution of 1 spike/second. MI between repetition rate and VS was evaluated in the same manner. VS values were calculated for each stimulus presentation to form distribution of VS values for each neuron for each trial. trials with non-significant VS values were assigned a MI value of zero bits/stimulus. In the case of ISI, the distribution of ISIs was calculated for each repetition rate, and linearly extrapolated to form a distribution with a resolution of 1ms.

Acknowledgements:

Funding: This research was funded by a Medical Research Council Grant (MR/M022889/1) and a European Research Council Starter Grant (CHIME) to DB. The funders had no role in study design, data collection and analysis, decision to publish, or preparation of the manuscript.

The authors thank Catherine Perrodin and James Cooke for comments and suggestions related to this manuscript.

bioRxiv preprint doi: https://doi.org/10.1101/661751; this version posted June 7, 2019. The copyright holder for this preprint (which was not certified by peer review) is the author/funder, who has granted bioRxiv a license to display the preprint in perpetuity. It is made available under aCC-BY-NC-ND 4.0 International license.

References

1. Peretz I, Zatorre RJ. Brain organization for music processing. Annu. Rev. Psychol. 2005; 56: 89–114. PMID: 15709930

2. Geiser E, Walker KM, Bendor D. Global timing: a conceptual framework to investigate the neural basis of rhythm perception in humans and non-human species. Frontiers in psychology. 2014; 5. doi: 10. 3389/fpsyg.2014.00005 PMID: 24478738

3. Rosen S. Temporal information in speech: acoustic, auditory and linguistic aspects. Philos. Trans. R. Soc. Lond. B Biol. Sci. 1992; 336, 367–373.

4. Large EW, Palmer C. Perceiving temporal regularity in music. Cognitive Science 2002; 26:1-37.

5. Singh NC, Theunissen FE. Modulation spectra of natural sounds and ethological theories of auditory processing. J. Acoust. Soc. Am. 2003; 114, 3394–3411.

6. De Ribaupierre F, Goldstein MH, Jr., Yeni-Komshian G. Cortical coding of repetitive acoustic pulses. Brain Res. 2003; 48: 205–225.

7. Gaese BH, Ostwald J. Complexity and temporal dynamics of frequency coding in the awake rat auditory cortex. Eur J Neurosci. 2003; 18: 2638–2652.

8. Lu T, Wang X. Temporal discharge patterns evoked by rapid sequences of wide- and narrowband clicks in the primary auditory cortex of cat. J Neurophysiol. 2000; 84: 236–246.

9. Lu, T, Liang L, Wang X. Temporal and rate representations of time-varying signals in the auditory cortex of awake primates. Nature Neuroscience 2000; 4:1131-1138.

10. Malone BJ, Scott BH, Semple MN. Dynamic amplitude coding in the auditory cortex of awake rhesus macaques. J Neurophysiol 2007; 98: 1451–1474.

11. Bendor D, Wang X. Differential neural coding of acoustic flutter within primate auditory cortex. Nat. Neurosci. 2007; 10, 763–771.

12. Sadagopan S and Wang X. Level Invariant Representation of Sounds by Populations of Neurons in Primary Auditory Cortex. J. Neurosci. 2008; 28: 3415-3426.

13. Stecker GC, Harrington IA, Middlebrooks JC. Location coding by opponent neural populations in the auditory cortex. PLoS Biol. 2005; 3(3):e78.

14. Romo R, Salinas E. Flutter discrimination: neural codes, perception, memory and decision making. Nat Rev Neurosci. 2003; 4(3):203-18.

15. Bendor D. The role of inhibition in a computational model of an auditory cortical neuron during the encoding of temporal information. PLoS Comput. Biol. 2015; 11, e1004197.

16. Gao L, Kostlan K, Wang Y, Wang X. Distinct Subthreshold Mechanisms Underlying Rate-Coding Principles in Primate Auditory Cortex. Neuron 2016; 91, 905919.

17. Wehr M, Zador AM. Balanced inhibition underlies tuning and sharpens spike timing in auditory cortex. Nature. 2003; 426(6965): 442–446.

18. Madison D, Nicoll R. Control of the repetitive discharge of rat CA1 pyramidal neurones in vitro. J Neurophysiol. 1984; 354: 319.

19. Tsodyks MV and Markram H. The Neural Code between Neocortical Pyramidal Neurons Depends on Neurotransmitter Release Probability. PNAS. 1997; 94, 719-723.

20. Phillips DP. Neural representation of sound amplitude in the auditory cortex: effects of noise masking. Behav Brain Res. 1990 Mar 26;37(3):197-214.

bioRxiv preprint doi: https://doi.org/10.1101/661751; this version posted June 7, 2019. The copyright holder for this preprint (which was not certified by peer review) is the author/funder, who has granted bioRxiv a license to display the preprint in perpetuity. It is made available under aCC-BY-NC-ND 4.0 International license.

21. Watkins PV and Barbour DL. Level-Tuned Neurons in Primary Auditory Cortex Adapt Differently to Loud versus Soft Sounds. Cereb Cortex. 2011 Jan; 21(1): 178–190.

22. Gao X, Wehr M. A coding transformation for temporally structured sounds within auditory cortical neurons. Neuron 2015; 86, 292–303.

23. De Ribaupierre F, Goldstein MH, Yeni-Komshian G. Intracellular study of the cat's primary auditory cortex. Brain research. 1972; 48: 185204.

24. Ojima H, Murakami K. Intracellular characterization of suppressive responses in supragranular pyramidal neurons of cat primary auditory cortex in vivo. Cerebral Cortex. 2002 ; 12(10): 10791091.

25. Zhou M, Liang F, Xiong XR, Li L, Li H, Xiao Z, et al. Scaling down of balanced excitation and inhibition by active behavioral states in auditory cortex. Nature neuroscience. 2014; 17(6): 842850.

26. David SV, Shamma SA. Integration over multiple timescales in primary auditory cortex. J Neurosci. 2013; 33:19154 19166

27. Joris PX, Schreiner CE, Rees A. Neural processing of amplitude-modulated sounds. Physiol. Rev. 2004; 84, 541577.

28. Kaas JH, Hackett TA. Subdivisions of auditory cortex and processing streams in primates. PNAS 2000; 97(22):11793-9.

29. Lemus L, Hernández A, Romo R. Neural codes for perceptual discrimination of acoustic flutter in the primate auditory cortex. PNAS 2009; 106(23), 9471–9476.

30. Mountcastle VB, Steinmetz MA, Romo R. Frequency discrimination in the sense of flutter: psychophysical measurements correlated with postcentral events in behaving monkeys. J Neurosci. 1990 Sep;10(9):3032-44.

31. Imaizumi K, Priebe NJ, Sharpee TO, Cheung SW, Schreiner CE. Encoding of Temporal Information by Timing, Rate, and Place in Cat Auditory Cortex. PLoS ONE 2010; 5(7): e11531.

32. Salinas E, Hernandez A, Zainos A, Romo R. Periodicity and firing rate as candidate neural codes for the frequency of vibrotactile stimuli. J. Neurosci. 2000; 20, 5503–5515.

33. Romo R, Salinas E. Flutter discrimination: neural codes, perception, memory and decision making. Nat Rev Neurosci. 2003; 4(3):203-18.

34. Atiani S, David V, Elgueda D, Locastro M, Radtke-Schuller S, Shamma SA, Fritz, J B. Emergent selectivity for task-relevant stimuli in higher-order auditory cortex. Neuron 2014; 82(2), 486–499.

35. Blackburn CC, Sachs MB. Classification of unit types in the anteroventral cochlear nucleus: PST histograms and regularity analysis. J Neurophysiol. 1989; 62(6):1303-29.

36. Frisina RD, Smith RL, Chamberlain SC. Encoding of amplitude modulation in the gerbil cochlear nucleus: II. Possible neural mechanisms. Hear Res. 1990; 44(2-3):123-41.

37. Wang X, Sachs MB. Neural encoding of single-formant stimuli in the cat II. Responses of anteroventral cochlear nucleus units. J Neurophysiol. 1994; 71:59–78.

38. Rhode WS and Greenberg SR. Encoding of amplitude modulation in the cochlear nucleus of the cat. J Neurophysiol. 1994; 71:1797-1825.

39. Langner G and Schreiner CE. Periodicity coding in the inferior colliculus of the cat. I. Neuronal mechanisms. J Neurophysiol. 1988; 60(6):1799-822.

40. Batra R, Kuwada S, Stanford TR. Temporal coding of envelopes and their interaural delays in the inferior colliculus of the unanesthetized rabbit. J Neurophysiol. 1989; 61:257–268.

41. Muller-Preuss P, Flachskamm C, Bieser A. Neural encoding of amplitude modulation within the auditory midbrain of squirrel monkeys. Hear Res. 1994; 80:197–208.

bioRxiv preprint doi: https://doi.org/10.1101/661751; this version posted June 7, 2019. The copyright holder for this preprint (which was not certified by peer review) is the author/funder, who has granted bioRxiv a license to display the preprint in perpetuity. It is made available under aCC-BY-NC-ND 4.0 International license.

42 Bartlett EL, Wang X. Neural Representations of Temporally-Modulated Signals in the Auditory Thalamus of Awake Primates. J Neurophysiol. 2007; 97:1005–1017.

43. Schreiner CE, Urbas JV. Representation of amplitude modulation in the auditory cortex of the cat. II Comparison between cortical fields. Hear Res. 1988; 32(1):49–63. [

44. Eggermont JJ. Rate and synchronization measures of periodicity coding in cat primary auditory cortex. Hear Res. 1991;56(1–2):153–67.

45. Eggermont JJ. Temporal modulation transfer functions for AM and FM stimuli in cat auditory cortex. Effects of carrier type, modulating waveform and intensity. Hear Res. 1994;74(1–2):51–66.

46. Rabang CF, Bartlett EL. A computational model of cellular mechanisms of temporal coding in the medial geniculate body (MGB). PloS one. 2011; 6(12): e29375.

47. Levy RB, Reyes AD. Coexistence of lateral and co-tuned inhibitory configurations in cortical networks. PLoS comput. biol. 2011; 7(10): e1002161.

48. Bendor, D., & Wang, X. (2008). Neural response properties of primary, rostral, and rostrotemporal core fields in the auditory cortex of marmoset monkeys. Journal of neurophysiology, 100(2), 888-906.

49. Bendor D, Wang X. Neural coding of periodicity in marmoset auditory cortex. J. Neurophysiol. 2010; 103(4):1809-22.

50. Kreeger L, Mehta P, Zemelman BV, Golding NL. Cholecystokinin neurons of the inferior colliculus provide direct and powerful excitation and inhibition to the medial geniculate body of the gerbil. 2018; Program No. 573.24. 2018 Neuroscience Meeting Planner. San Diego, CA: Society for Neuroscience.

51. Tsodyks MV, Markram H. Plasticity of neocortical synapses enables transitions between rate and temporal coding. Lect. Notes Comput. Sci., 1996; 1112,445450.

52. Abbott LF, Varela JA, Sen K, Nelson SB. Synaptic depression and cortical gain control. Science 1997; 275, 220224.

53. Dayan P and Abbott LF. Theoretical Neuroscience: Computational and Mathematical Modeling of Neural Systems. The MIT Press 2005.

54. Strong SP, Koberle R, van Steveninck RRD, Bialek W. Entropy and information in neural spike trains. Phys Rev Let 1998; 80: 197–200.

55. Cliff AD, Ord JK. Spatial autocorrelation. London: Pion. 1973; 178 p.

Supporting information

S1 Fig. Adaptation to stimulus pulse trains in Sync+ and Sync- neurons. For all neurons, we calculated the difference in normalized firing rate between the first and last acoustic pulse for a given stimulus. (a.) For Sync- neurons, this difference was significative for all repetition rates (Wilcoxon signed rank test, $P << 0.001$) with the exception of 8Hz (Wilcoxon signed rank test, $P = 0.10$). For Sync + neurons, this difference was significative for repetition rates equal or larger than 16Hz, with the exception of 40Hz (8Hz; $P = 0.71$. 12Hz; $P = 0.06$. 16Hz; $P = 0.007$. 20Hz; $P = 0.04$. 24Hz; $P = 0.009$. 28Hz; $P = 0.006$. 32Hz; $P = 0.002$. 36Hz; $P = 0.01$. 40Hz; $P = 0.07$. 44Hz; $P = 0.03$. 48Hz; $P = 0.04$). (b.) We then compared this difference between Sync+ and Sync- neuron populations ($n = 26$ and $n = 27$ respectively). This difference was significant for repetition rates above 20 Hz. (Wilcoxon rank-sum test. 8Hz; $P = 0.37$. 12Hz; $P = 0.61$. 16Hz; $P = 0.12$. For higher repetition rates $P << 0.01$)

S2 Fig. Sync+ (a.) and Sync- (b.) neuron responses to stimulus pulse trains. For all neurons, the average number of spikes were extracted at each acoustic pulse for all repetition rates. The responses were then normalized by average discharge rate of the neuron during stimulus presentation. Real data (grey), linear fit (red) first degree exponential fit (blue).

bioRxiv preprint doi: https://doi.org/10.1101/661751; this version posted June 7, 2019. The copyright holder for this preprint (which was not certified by peer review) is the author/funder, who has granted bioRxiv a license to display the preprint in perpetuity. It is made available under aCC-BY-NC-ND 4.0 International license.

S3 Fig. Fitted model coefficients to adaptation during stimulus presentation. (a, b) linear model coefficients with 95% confidence intervals. Stronger negative values of p1 indicate stronger depression during stimulus presentation. (c.) R-squared fit of data to linear model. (c, d) exponential model coefficients with 95% confidence intervals. Stronger negative values of b indicate a steeper curve to the exponential model, indicating a fast adaptation followed by a flat response. Positive values of b indicate no adaptation or facilitation.

S4 Fig. Onset response amplitude relative to strength of adaptation. Average onset response at time constants $\{\tau_{pE} = 0.15, \tau_{pI} = 0.10\}$ for different values of A_{DE} and A_{DI}. Onset response amplitude did not vary with strength of adaptation.

S5 Fig. Comparison of ISI after stimulus onset. ISIs between the first four spikes were compared to determine the presence of SRA for Sync+ (a,b) and Sync- (c,d) real neuron populations for all individual trials across all neurons (n =260 and n = 270 respectively). All four distributions had a non-zero median (KS test, $P < 0.05$). For Sync+ neurons, the median difference between first and second ISI was 0.59s (a.) and was 1.21ms for the median difference between first and third ISI (b.). For Sync- neurons, the median difference between first and second ISI was 0.33s (c.) and was 0.24ms for the median difference between first and third ISI (d.).

S6 Fig. Monotonicity and adaptation in individual neurons. (a). correlation between adaptation and firing rate. Distribution of strength of adaptation near onset (b.) and at the middle of stimuli duration (c.) Sync- neurons showed significant depression between the first and second (median = 0.73, t-test, $P << 0.001$) and between first and third pulse (median = 0.90, $P << 0.001$) (b.), but not between 2nd and 5th pulse nor between 5th and 8th pulse (median = -0.12, P = 0.33 and median = 0.07, P = 0.51 respectively.) (c.). Sync + neurons showed no significant depression between 1st and 2nd pulses and between 1st and 3rd pulses respectively (median = 0 for both, t-test, P = 0.12 and P = 0.25 respectively) nor at the later stages of stimuli presentation between 2nd and 5th pulse (median = -0.33, p value = 0.31), and between 5th and 8th pulse, (median = 0.07 p value = 0.54).

S7 Fig. Puretone responses. (a.) Average firing rate for simulated Sync+ and Sync- responses to puretones. (b.) Average firing rate for real Sync + (n = 26) and Sync- (n = 27) neurons to puretones.

S8 Fig. Puretone responses and SFA. Puretone responses in simulated Sync+ (a.) and Sync- (b.) neurons. SFA was introduced to our model with values ranging between 10 and 50nS (see methods). Stronger SFA reduced both onset and sustained responses on Sync+ model neurons but did not affect Sync- neurons. (c.) Average of median spike times during stimuli presentation for simulated neurons with different values of adaptation amplitude A_D.

bioRxiv preprint doi: https://doi.org/10.1101/661751; this version posted June 7, 2019. The copyright holder for this preprint (which was not certified by peer review) is the author/funder, who has granted bioRxiv a license to display the preprint in perpetuity. It is made available under aCC-BY-NC-ND 4.0 International license.

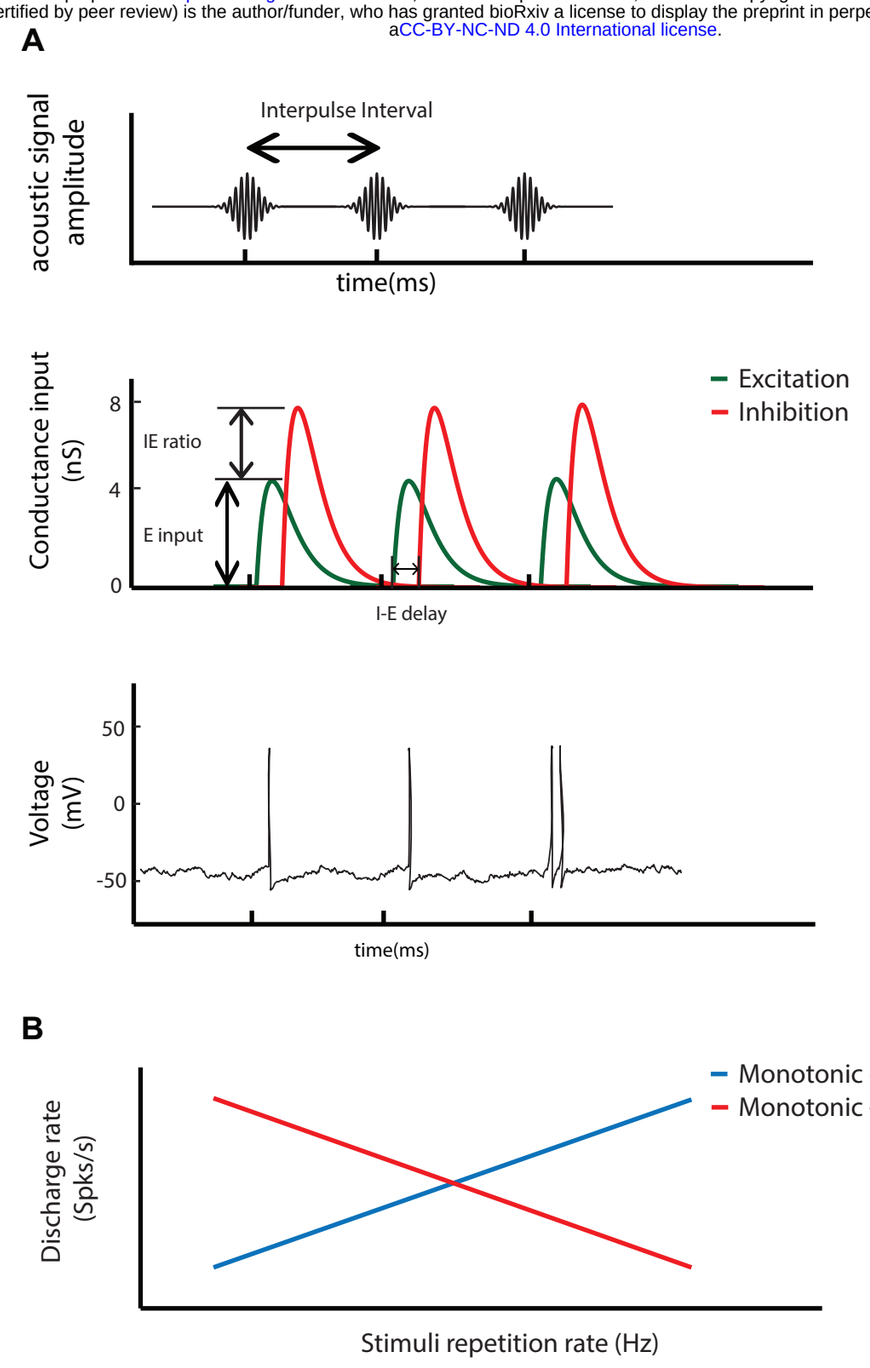

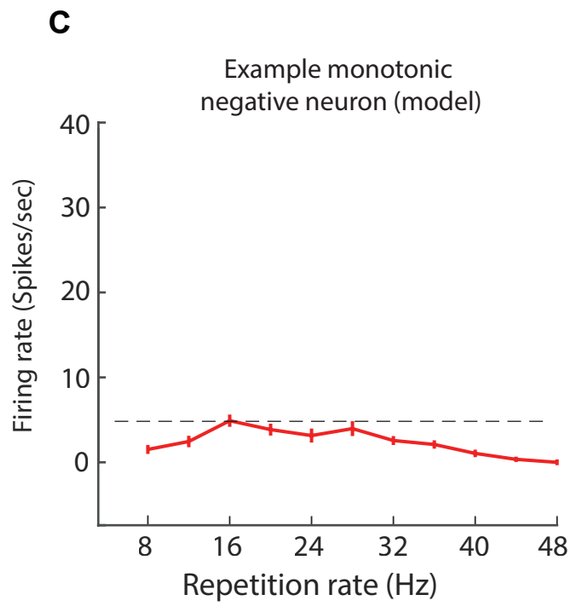

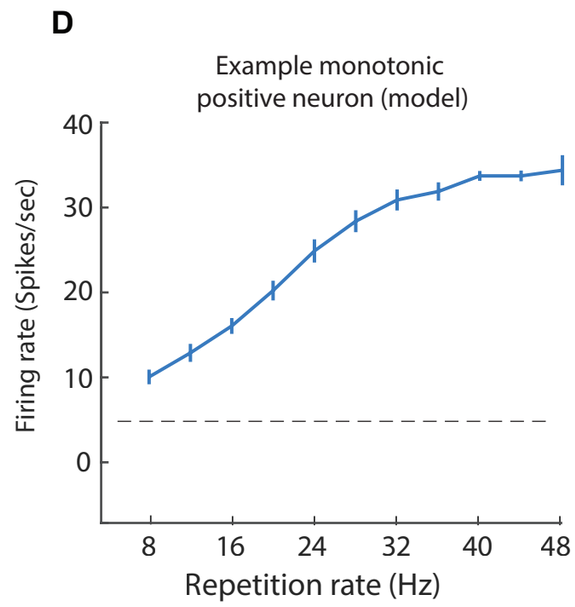

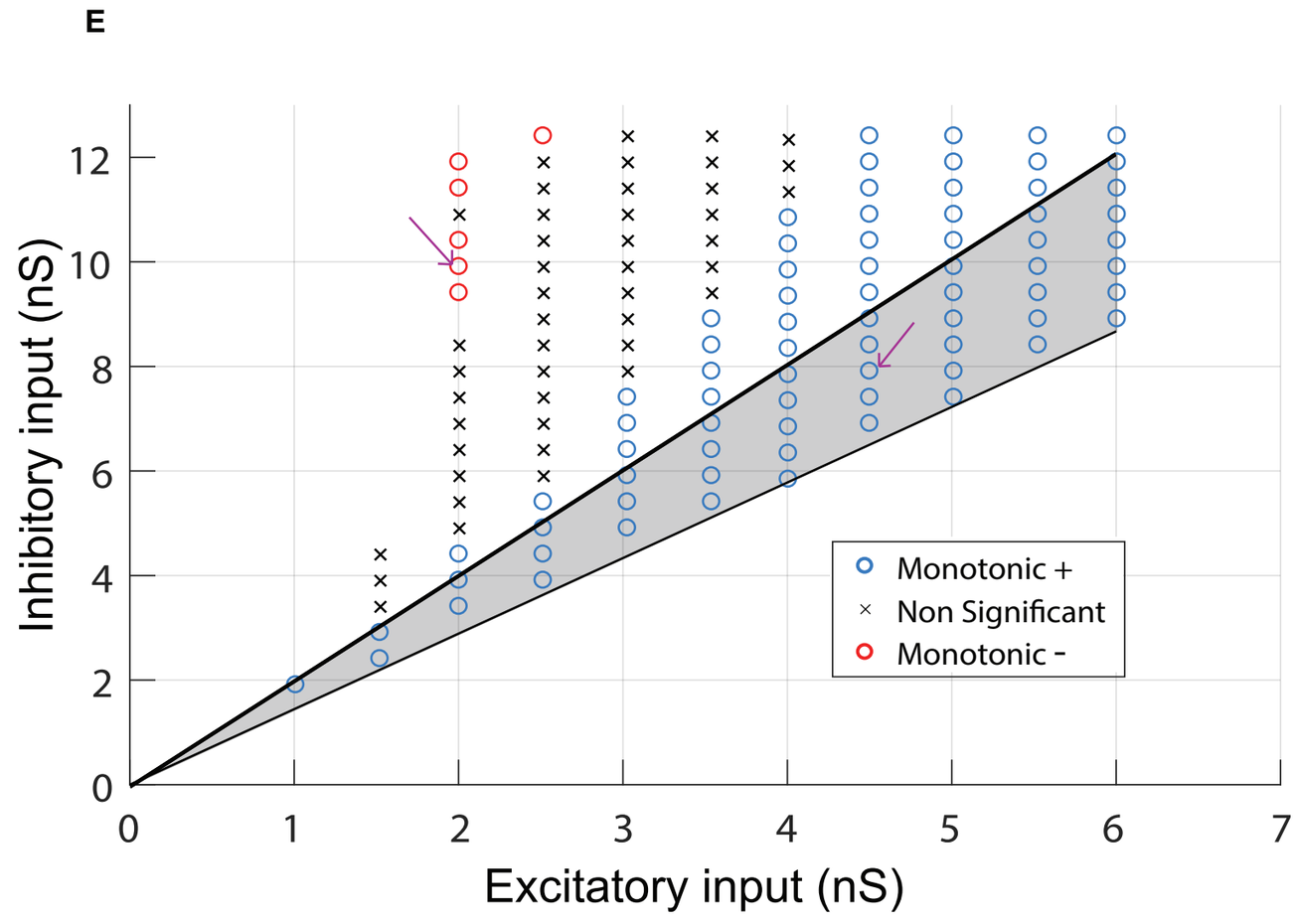

Figure1. Computational model of an auditory cortical neuron

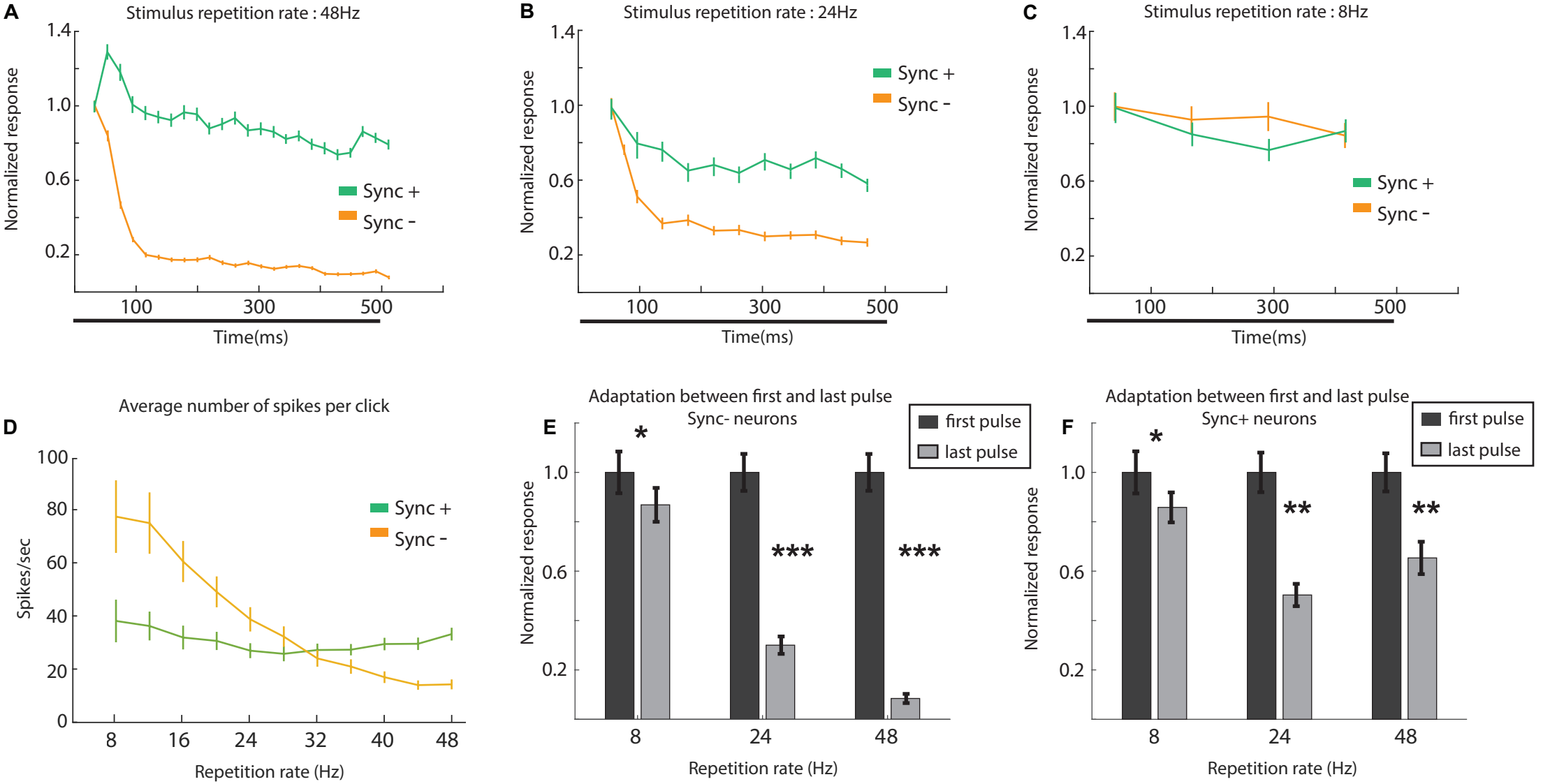

Figure 2. Event-related activity of monotonic Sync neurons

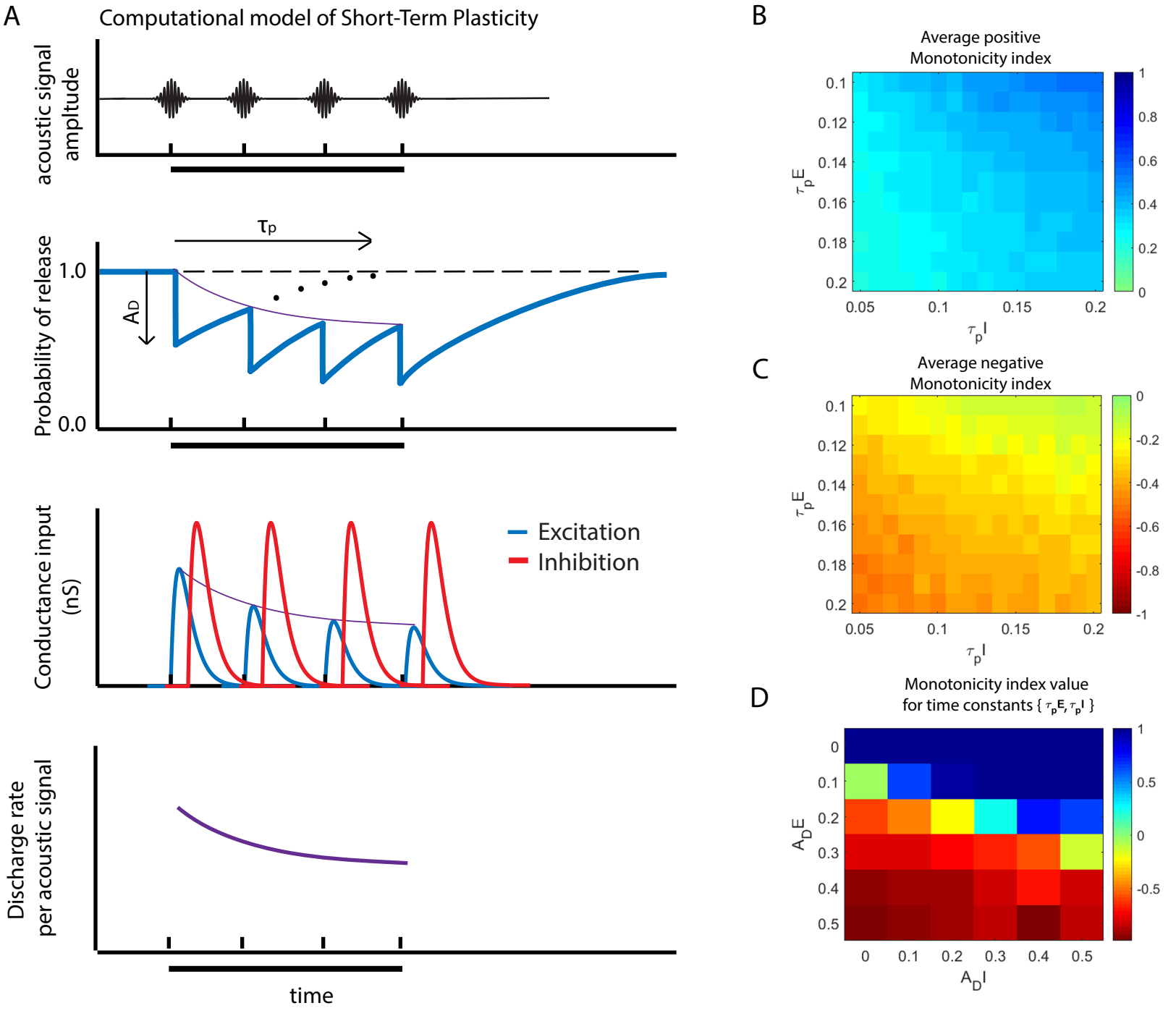

Figure3. Computational model of an auditory cortical neuron with short term depression

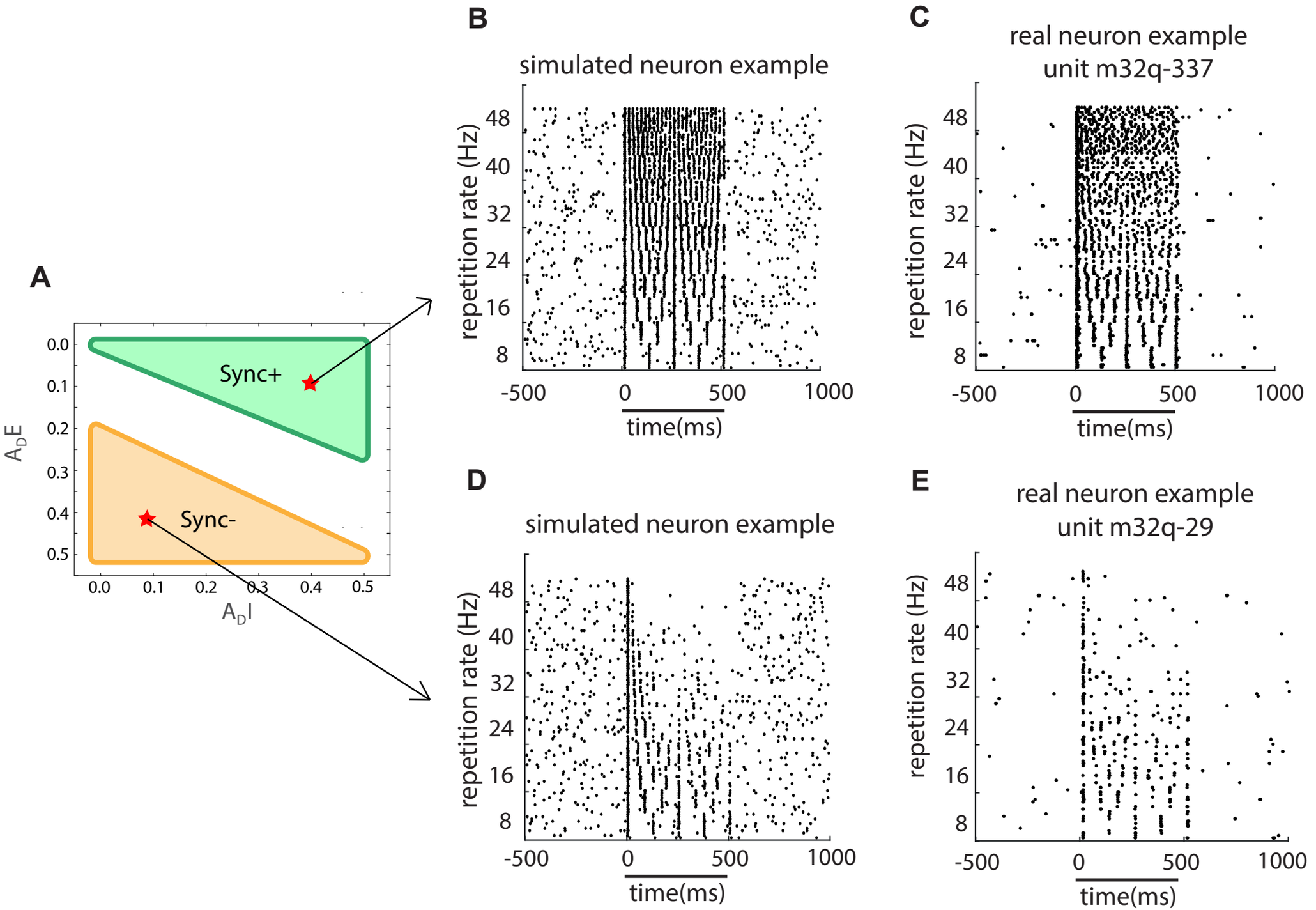

Figure 4. Real and Simulated monotonic Sync example neurons

bioRxiv preprint doi: https://doi.org/10.1101/661751; this version posted June 7, 2019. The copyright holder for this preprint (which was not certified by peer review) is the author/funder, who has granted bioRxiv a license to display the preprint in perpetuity. It is made available under aCC-BY-NC-ND 4.0 International license.

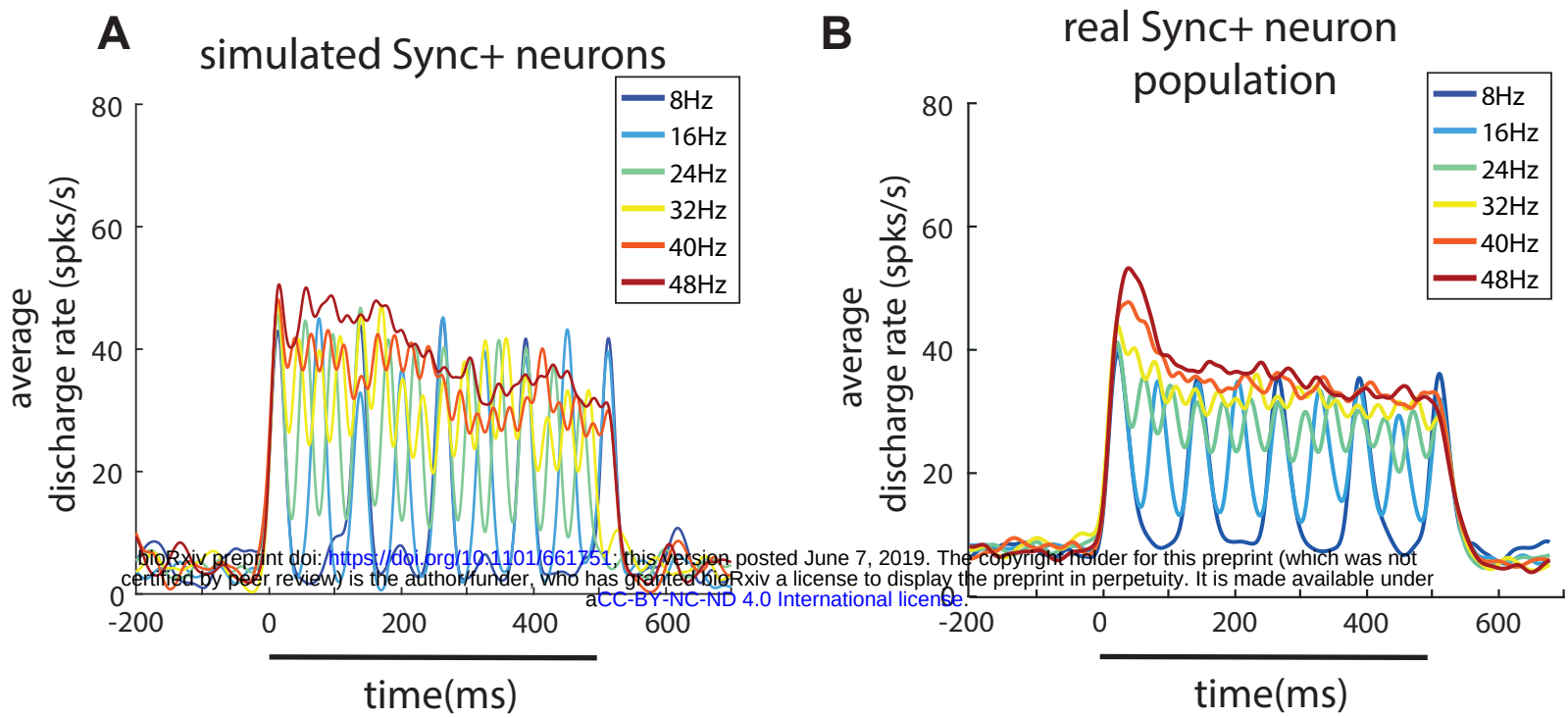

Figure 5. Monotonicity of real and simulated neurons

bioRxiv preprint doi: https://doi.org/10.1101/661751 this version posted June 7, 2019. The copyright holder for this preprint (which was not certified by peer review) is the author/funder, who has granted bioRxiv a license to display the preprint in perpetuity. It is made available under aCC-BY-NC-ND 4.0 International license.

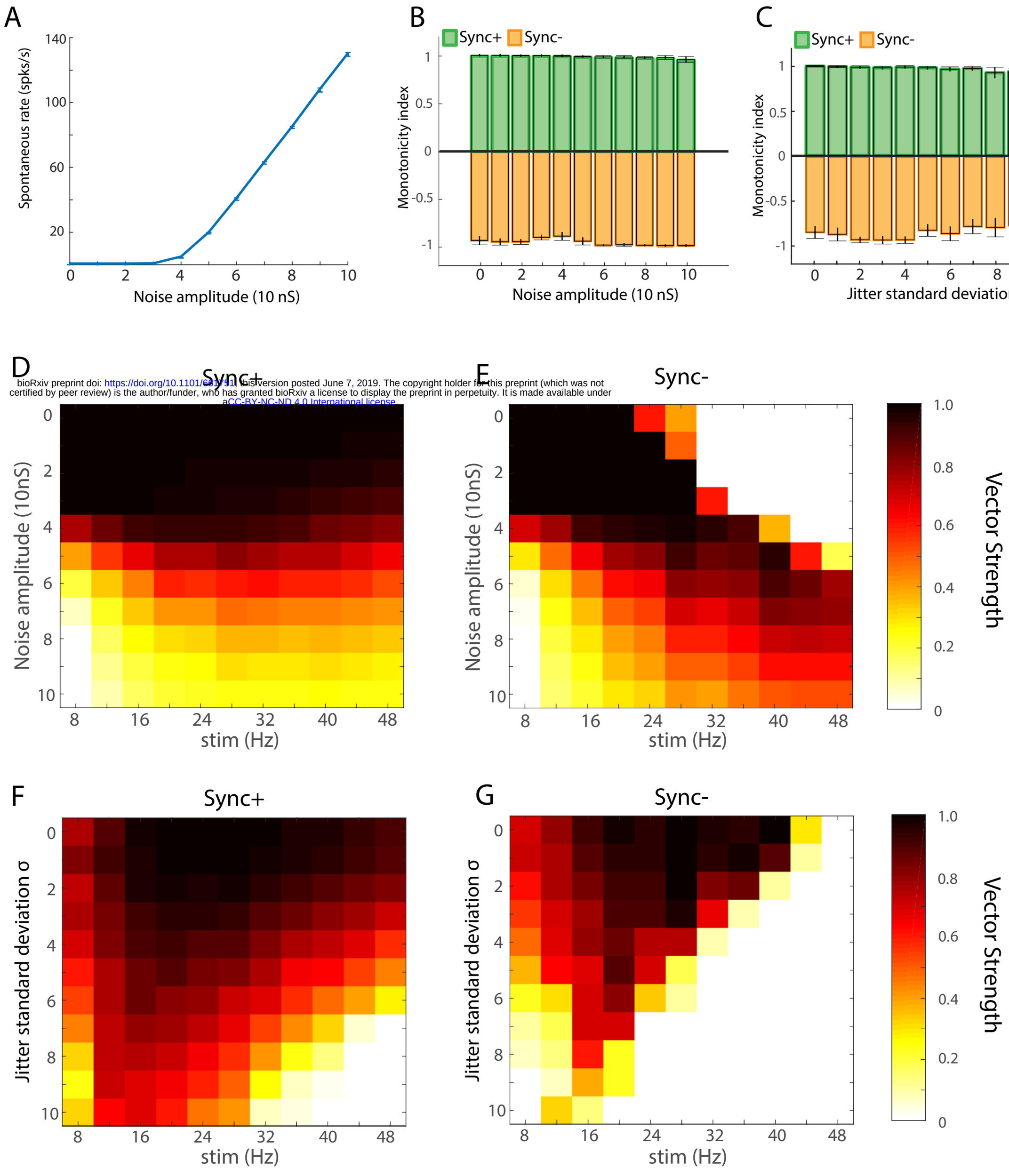

Figure 6. Model robustness

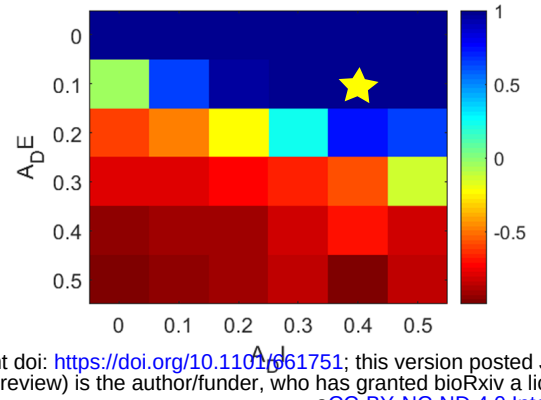

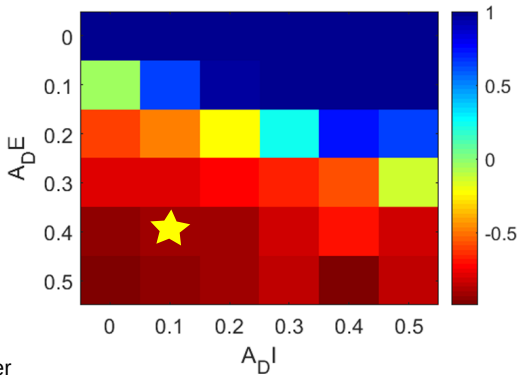

bioRxiv preprint doi: https://doi.org/10.1101/661751; this version posted June 7, 2019. The copyright holder for this preprint (which was not certified by peer review) is the author/funder, who has granted bioRxiv a license to display the preprint in perpetuity. It is made available under aCC-BY-NC-ND 4.0 International license.

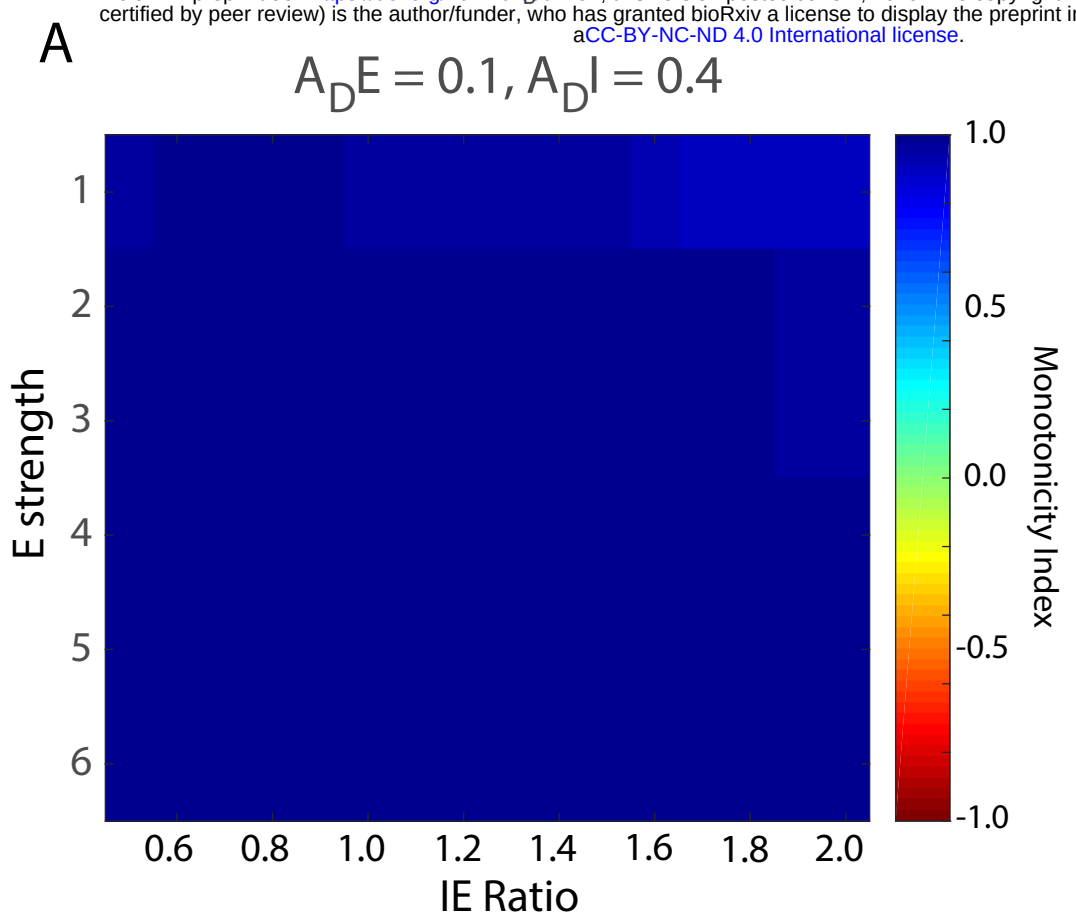

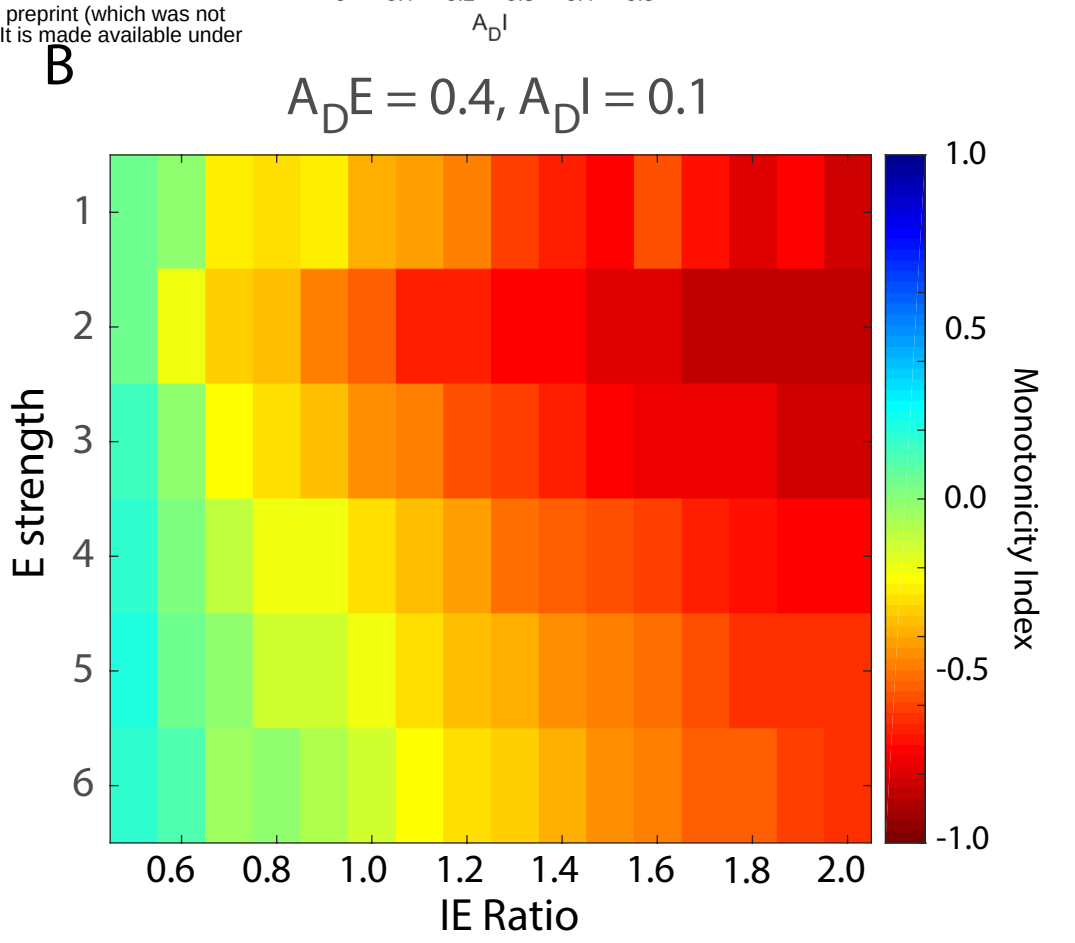

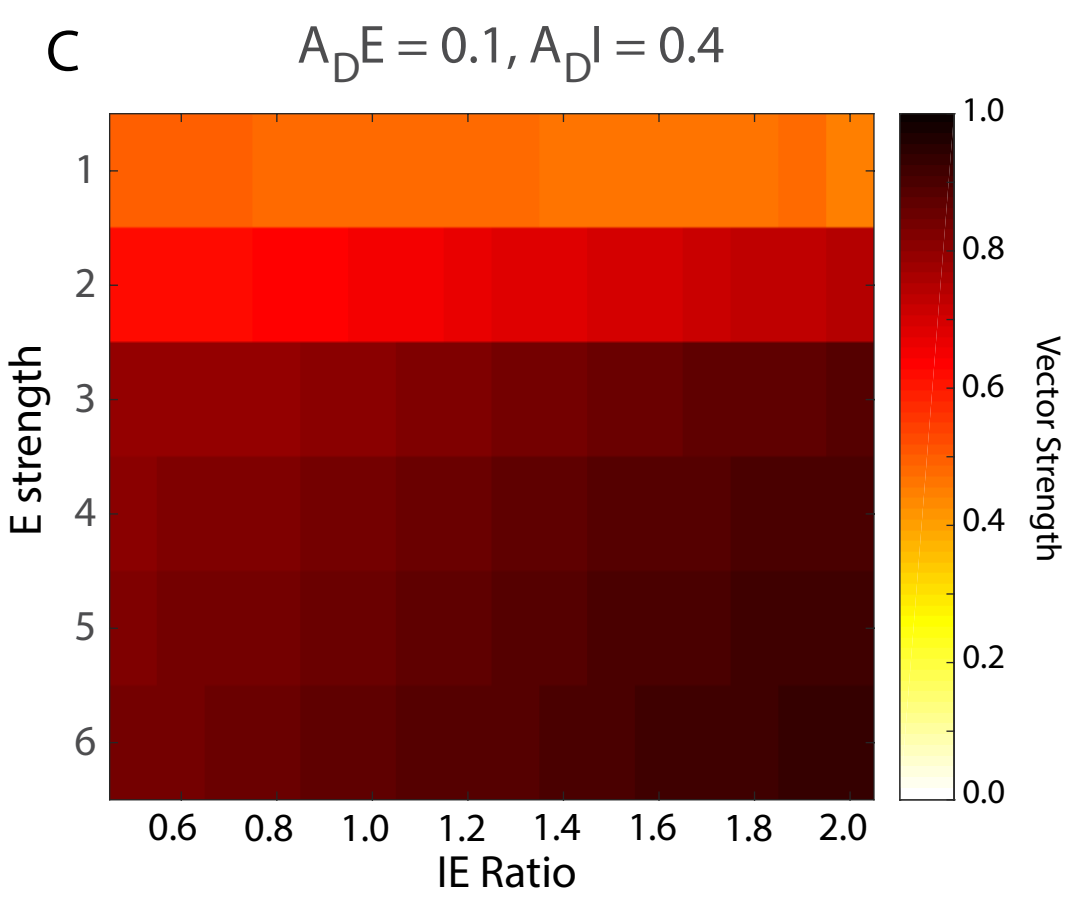

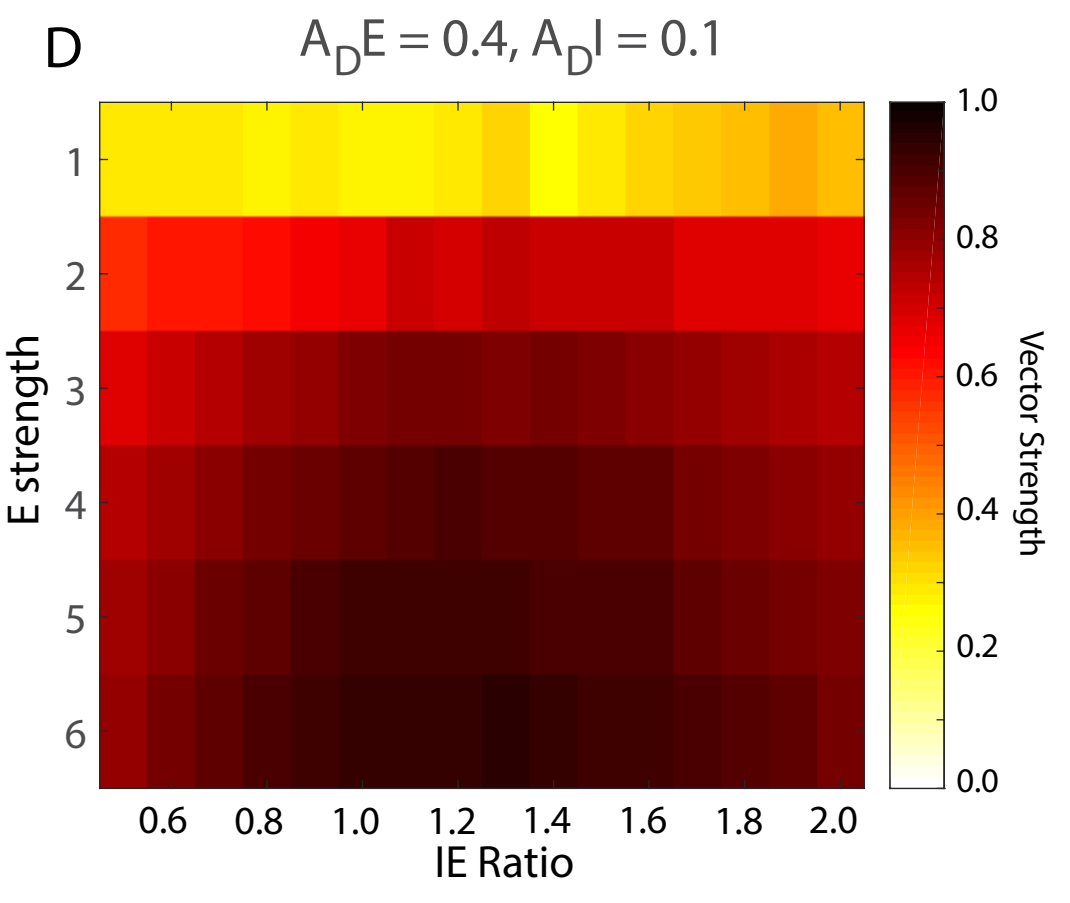

Figure 7. Model robustness regarding Excitation and Inhibition amplitude

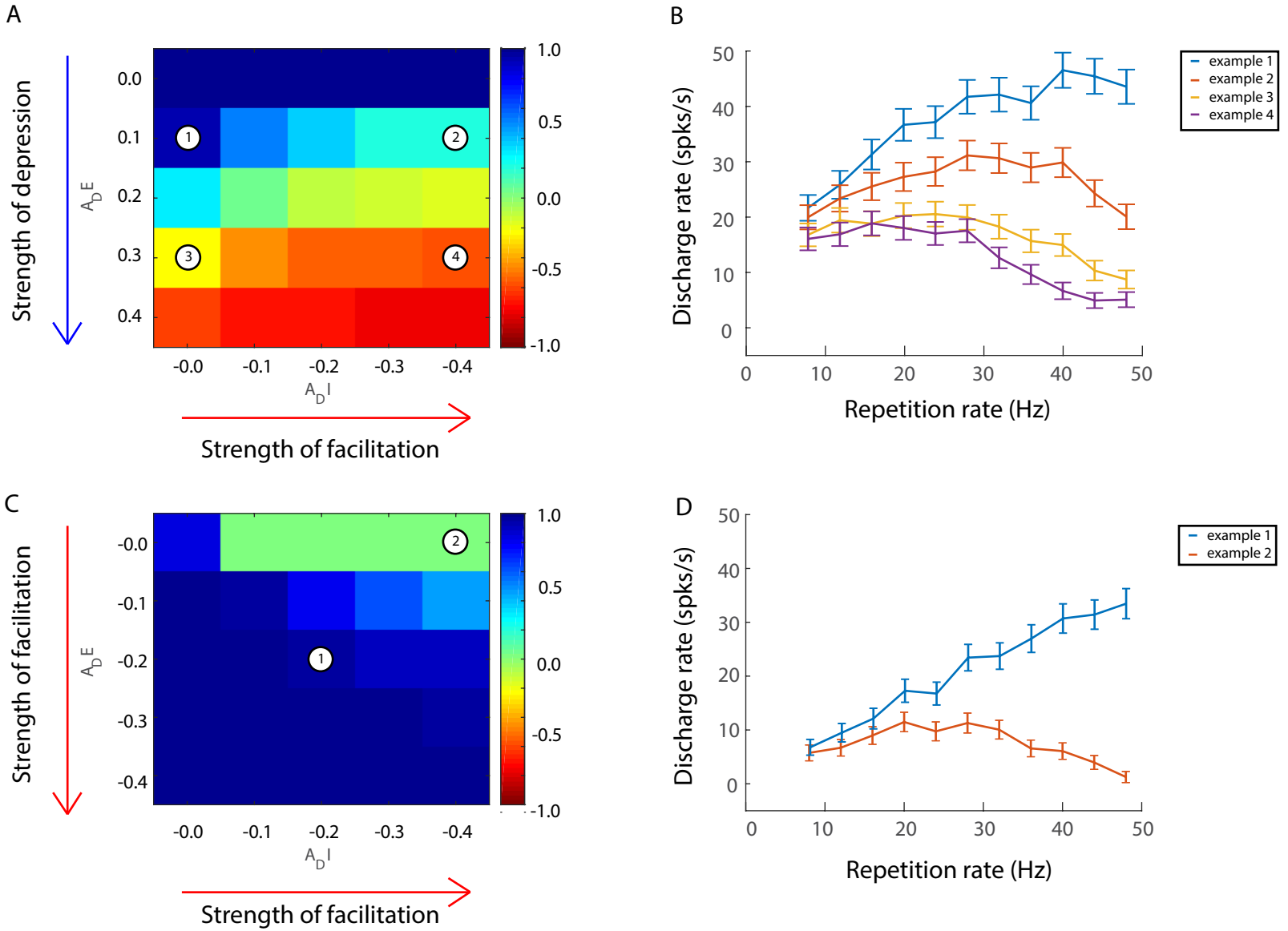

Figure 8. Computational model including short term facilitation

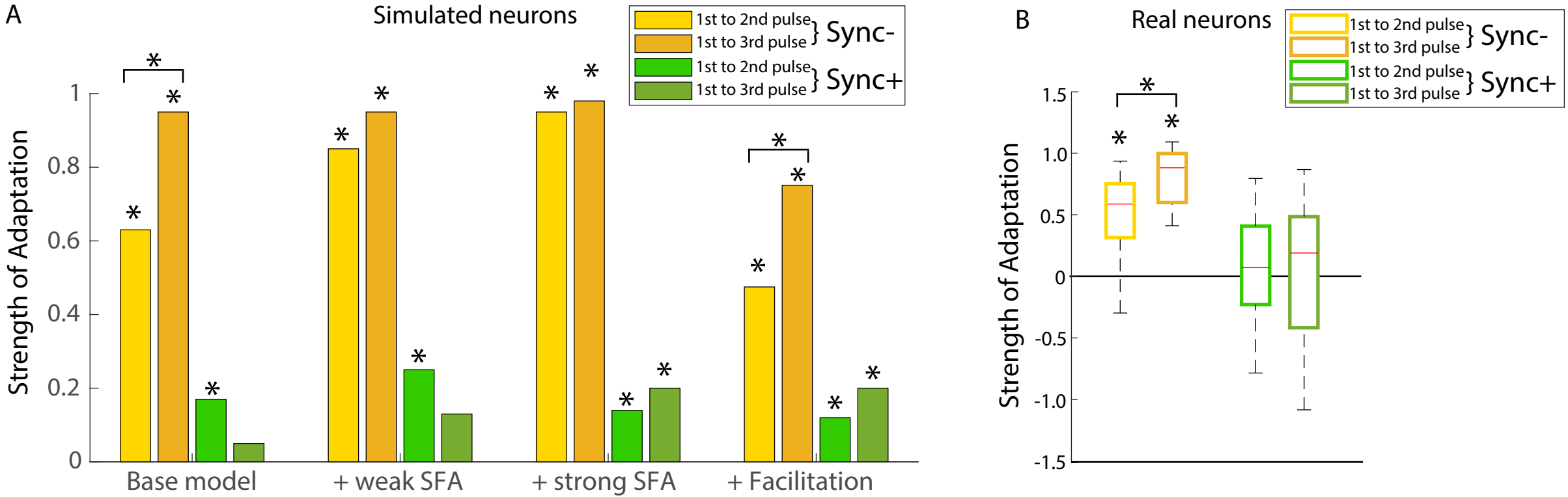

Figure 9. Adaptation between individual synaptic inputs for real neurons and different models

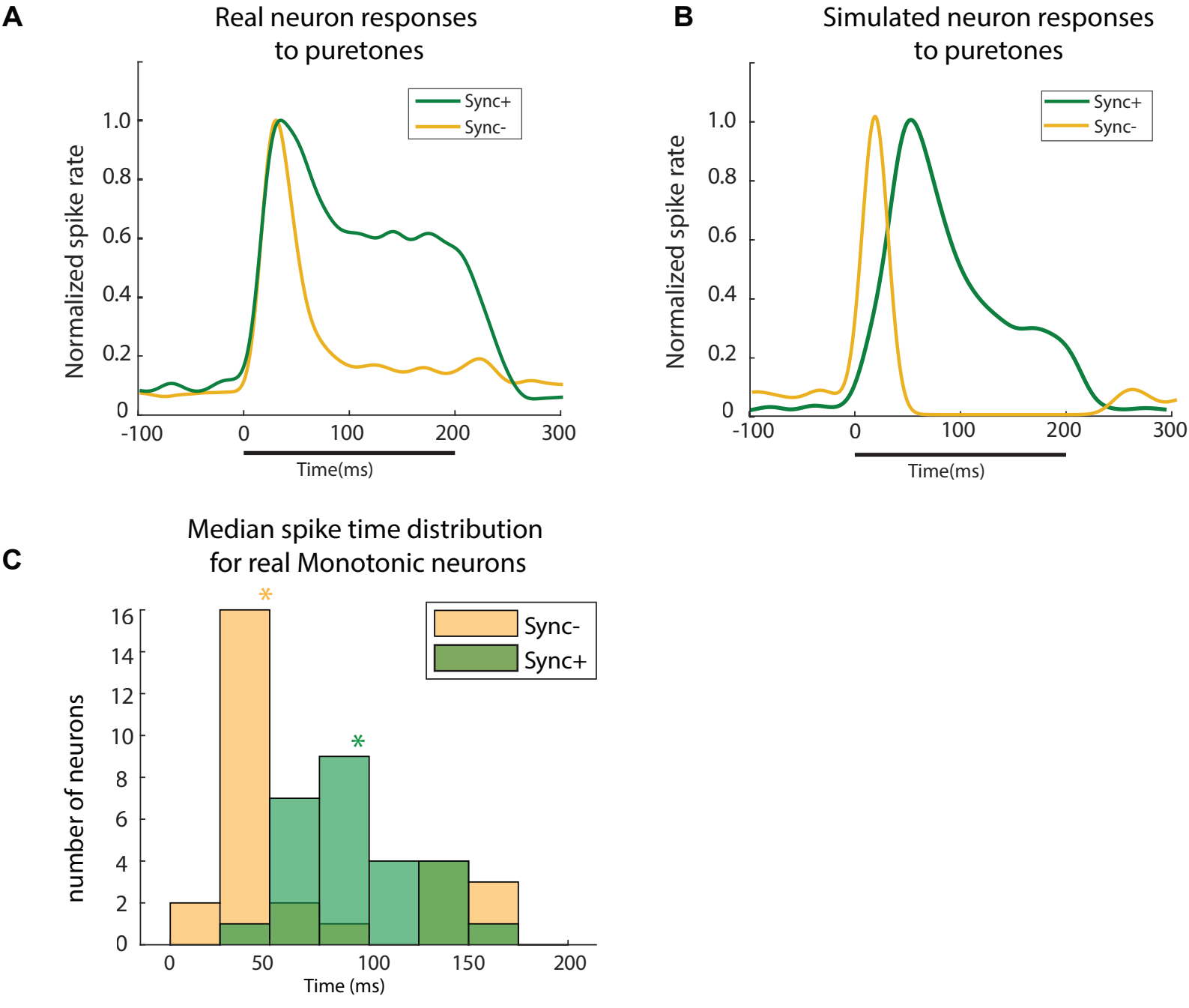

Figure 10. Pure tone responses

bioRxiv preprint doi: https://doi.org/10.1101/661751; this version posted June 7, 2019. The copyright holder for this preprint (which was not certified by peer review) is the author/funder, who has granted bioRxiv a license to display the preprint in perpetuity. It is made available under aCC-BY-NC-ND 4.0 International license.

Figure 11. Opponent coding with Sync+ and Sync- neurons.

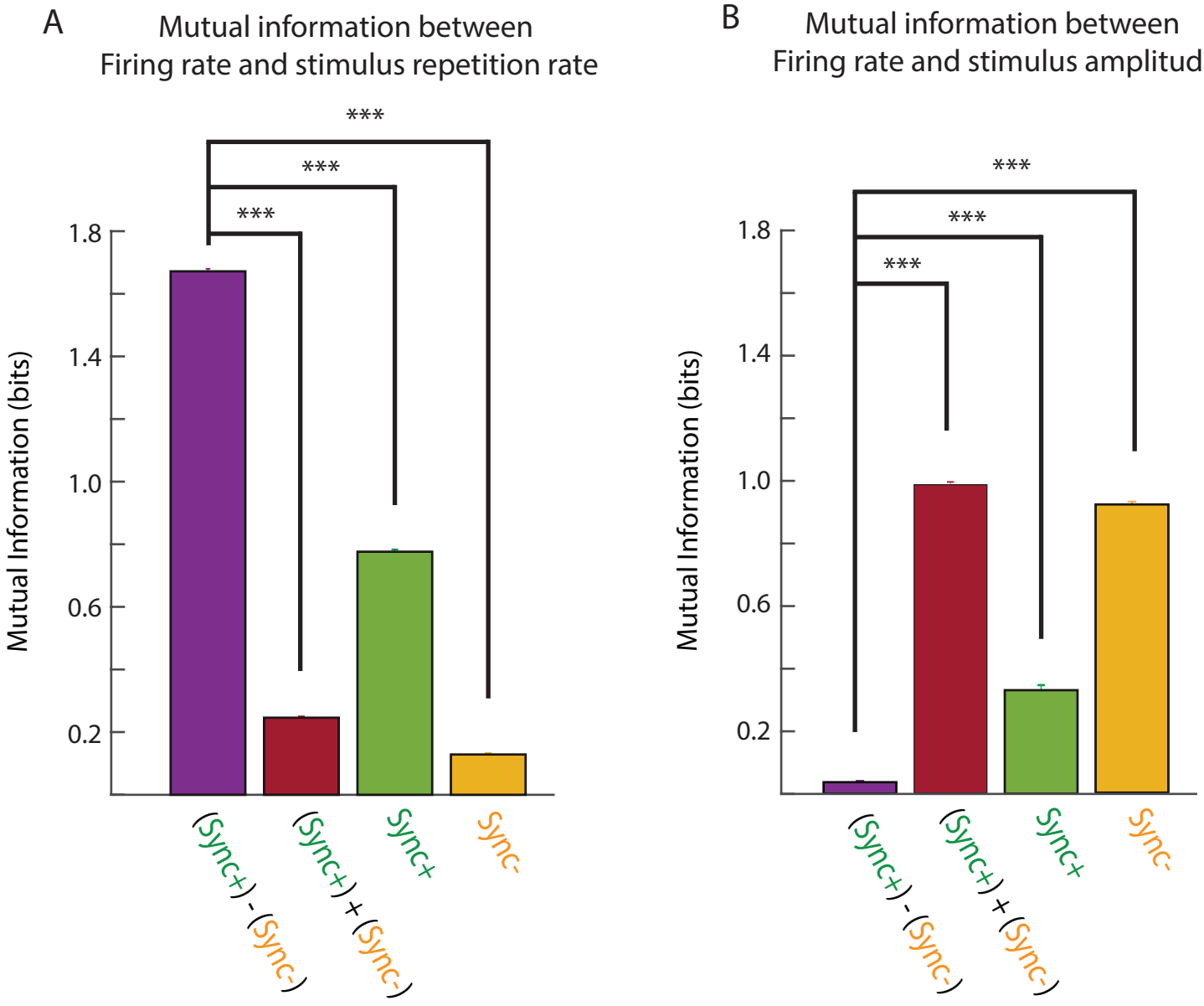

Figure12. Mutual information and opponent coding